The graphite deposit at Borrowdale (UK): A catastrophic mineralizing event associated with Ordovician magmatism

L. Ortega [a], D. Millward [b], F.J. Luque [a,*], J.F. Barrenechea [a], O. Beyssac [c], J.-M. Huizenga [d], M. Rodas [a], S.M. Clarke [b,1]

[a] *Dpto. Cristalografía y Mineralogía, Facultad de Geología, Universidad Complutense de Madrid, 28040 Madrid, Spain*
[b] *British Geological Survey, Murchison House, West Mains Road, Edinburgh EH9 3LA, UK*
[c] *Laboratoire de Géologie, CNRS, Ecole Normale Supérieure, 24 rue Lhomond, 75005 Paris, France*
[d] *School of Environmental Science and Development, North-West University, Potchefstroom, South Africa*

Abstract

The volcanic-hosted graphite deposit at Borrowdale in Cumbria, UK, was formed through precipitation from C–O–H fluids. The $\delta^{13}C$ data indicate that carbon was incorporated into the mineralizing fluids by assimilation of carbonaceous metapelites of the Skiddaw Group by andesite magmas of the Borrowdale Volcanic Group. The graphite mineralization occurred as the fluids migrated upwards through normal conjugate fractures forming the main subvertical pipe-like bodies. The mineralizing fluids evolved from CO_2–CH_4–H_2O mixtures ($XCO_2 = 0.6$–0.8) to CH_4–H_2O mixtures. Coevally with graphite deposition, the andesite and dioritic wall rocks adjacent to the veins were intensely hydrothermally altered to a propylitic assemblage. The initial graphite precipitation was probably triggered by the earliest hydration reactions in the volcanic host rocks. During the main mineralization stage, graphite precipitated along the pipe-like bodies due to $CO_2 \rightarrow C + O_2$. This agrees with the isotopic data which indicate that the first graphite morphologies crystallizing from the fluid (cryptocrystalline aggregates) are isotopically lighter than those crystallizing later (flakes). Late chlorite–graphite veins were formed from CH_4-enriched fluids following the reaction $CH_4 + O_2 \rightarrow C + 2H_2O$, producing the successive precipitation of isotopically lighter graphite morphologies. Thus, as mineralization proceeded, water-generating reactions were involved in graphite precipitation, further favouring the propylitic alteration. The structural features of the pipe-like mineralized bodies as well as the isotopic homogeneity of graphite suggest that the mineralization occurred in a very short period of time.

1. INTRODUCTION

Most of the highest quality natural graphite used in industrial applications occurs as veins that crosscut their host rocks and therefore can be regarded as epigenetic. This category includes deposits of both current and past economic interest (e.g. Sri Lanka, India, New York, Montana, etc.). In such occurrences graphite is found along fracture systems and it is usually deposited from carbon-bearing fluids. In spite of the economic significance of this type of graphite deposit, little is known about the composition and characteristics of the fluids responsible for its formation. Thus, although fluid inclusions provide unique and direct information about the fluids involved in mineralization processes, there is only one reference on fluid inclusion studies in graphite deposits dealing with quartz–graphite veins hosted by metasedimentary rocks (Duke et al., 1990). More recently, Satish-Kumar (2005) has confirmed the usefulness of fluid inclusion studies to infer the mechanism of graphite precipitation and to model the carbon isotope evolution of the fluid–graphite system in granulites.

* Corresponding author.
E-mail address: jluque@geo.ucm.es (F.J. Luque).
[1] Present address: School of Physical and Geographical Sciences, Keele University, Keele ST5 5BG, UK.

This paper characterizes the deposit at Seathwaite in Borrowdale, Cumbria (UK), where graphite was discovered. Mining there began at least as early as the late 16th century, and continued until the late 19th century, producing material for the casting of cannonballs, for coin moulds and as the basis for the renowned Keswick pencil industry. In addition to the historical interest of this deposit, it is also one of the only two large graphite occurrences known worldwide to be hosted by volcanic rocks, the other being that of Huelma in southern Spain (Barrenechea et al., 1997).

The origin of the Borrowdale graphite deposit has proved controversial, although even the earliest studies suggested the derivation from the assimilation of metapelitic rocks (Ward, 1876). Strens (1965) stated that graphite derived from the breakdown of carbon monoxide in the magmatic gases promoted by iron-bearing minerals. Later, the deposit was regarded as epigenetic and graphite was considered to be derived from the assimilation of sedimentary organic matter (Weis et al., 1981). Parnell (1982) pointed to the relationship with granite intrusion in this area which promoted the mobilization of organic carbon compounds and the graphite mineralization. More recent works (Luque et al., 1998; Lindgren and Parnell, 2006) attributed the origin of the deposit to precipitation from carbon-bearing fluids. Luque et al. (2009) concluded that this is the first known volumetrically large fluid-deposited graphite occurrence formed at moderate temperature in which graphite displays high crystallinity. In addition, the textural sequence of graphite morphologies and their isotopic analyses suggest precipitation from fluids with supersaturation in carbon decreasing progressively and the organic origin of the carbon in the mineralizing fluids (Barrenechea et al., 2009).

The aim of this work is to unravel the processes that led to the formation of this unique deposit. This paper integrates field evidence with new data from a fluid inclusion study and with the mineralogical and isotopic results from both the graphite deposit and its inferred carbon source (Skiddaw Group metapelites). Such an approach has provided a further insight into the progress of the mineralizing event and therefore a tool for understanding the mineralization processes in other fluid-deposited graphite occurrences.

2. GEOLOGIC BACKGROUND

The Borrowdale graphite deposit (Cumbria, UK) is hosted by andesite lavas and sills belonging to the Upper Ordovician (Katian) Borrowdale Volcanic Group (BVG), and by a probably contemporaneous hypabyssal dioritic intrusion (Fig. 1). The host BVG was emplaced during a brief magmatic episode that lasted no longer than 5 Ma (Millward and Evans, 2003). The subaerial, 6000 m-thick, caldera-related succession comprises basaltic to rhyolitic lavas, sills, and pyroclastic rocks of medium- to high-K calc-alkaline, continental-margin, affinity (Beddoe-Stephens et al., 1995; Millward and Evans, 2003; Millward, 2004). The volcanic rocks are underlain by the upper Cambrian to Middle Ordovician Skiddaw Group, a succession of marine turbiditic mudstones and sandstones at least 5000 m thick (Cooper et al., 1995, 2004; Stone et al., 1999). Granitic plutons associated with the Caradoc volcanism intrude the Skiddaw and Borrowdale Volcanic Groups, and are inferred to be linked to a granitic batholith concealed at a shallow depth (<4 km) beneath both groups (Lee, 1986). Clay mineral assemblages developed in the Skiddaw Group are consistent with early, very low-grade metamorphism related to sedimentation and burial in an extensional basin where heat flow was quite high, possibly in the range 35–50 °C/km, and related to extensional, high heat-flow associated with volcanism and granitic batholith emplacement (Fortey, 1989; Fortey et al., 1993). Subsequent closure of the basin caused tectonic thickening with associated anchizonal to epizonal metamorphism (Soper and Woodcock, 2003; Merriman, 2006).

The following three lines of evidence suggest that the Skiddaw Group rocks have contributed to the geochemical development of later aspects of Lake District geology. First, the presence of garnet phenocrysts in peraluminous rocks in the BVG and associated intrusions (Fitton, 1972) and the Sm–Nd isotope geochemistry of the rocks have been attributed to assimilation of pelitic material, most likely from the Skiddaw Group (McConnell et al., 2002). Second, sulphur isotope data from sulphides within the andesite rocks of the BVG also support this contention (Lowry et al., 1991). Finally, a zone of intense metasomatic alteration of the Skiddaw Group rocks in the northern Lake District is depleted in many of the elements (mainly Ni, S, Zn, C, Cu, and Fe, among others) that are concentrated in the varied mineral deposits of the Lake District, suggesting that these rocks could be the source of the carbon (Cooper et al., 1988). Metasomatic alteration is thought to be related to a concealed Acadian (ca. 400 Ma) granitic intrusion (Cooper et al., 1988).

The age of graphite emplacement is poorly defined. The whole-rock and chlorite mineral-separate K–Ar ages of 382 and 376 Ma for the intrusion and vein deposit, respectively (Mitchell and Ineson, 1975), are considered to have been reset like many others from the Lake District that have been determined by this method (Stone et al., 1999). A pre-Early Devonian age for the deposit is suggested by the presence of a pronounced Acadian cleavage in many hand specimens from the mine spoil heaps, but this fabric could not be traced in situ in the mine from the veins into the wall rock. The apparently direct association of the graphite with emplacement of the dioritic intrusion lead Millward (2004) to infer that the deposit was emplaced during Ordovician time; with the exception of the suite of Early Devonian lamprophyre dykes, all mafic intrusions in the Lake District are considered to have an age of about 450 Ma (Katian).

3. MATERIALS AND ANALYTICAL METHODS

Samples from the graphite ore bodies, their volcanic host rocks and from the Skiddaw Group were studied in polished thin sections with a Zeiss Axiophot microscope under both transmitted and reflected light. Samples of graphite and the volcanic host rocks were collected along three of the old mine levels, that is, Gill's, Gilbert's and Farey's, and along the Grand Pipe (Fig. 2). In addition,

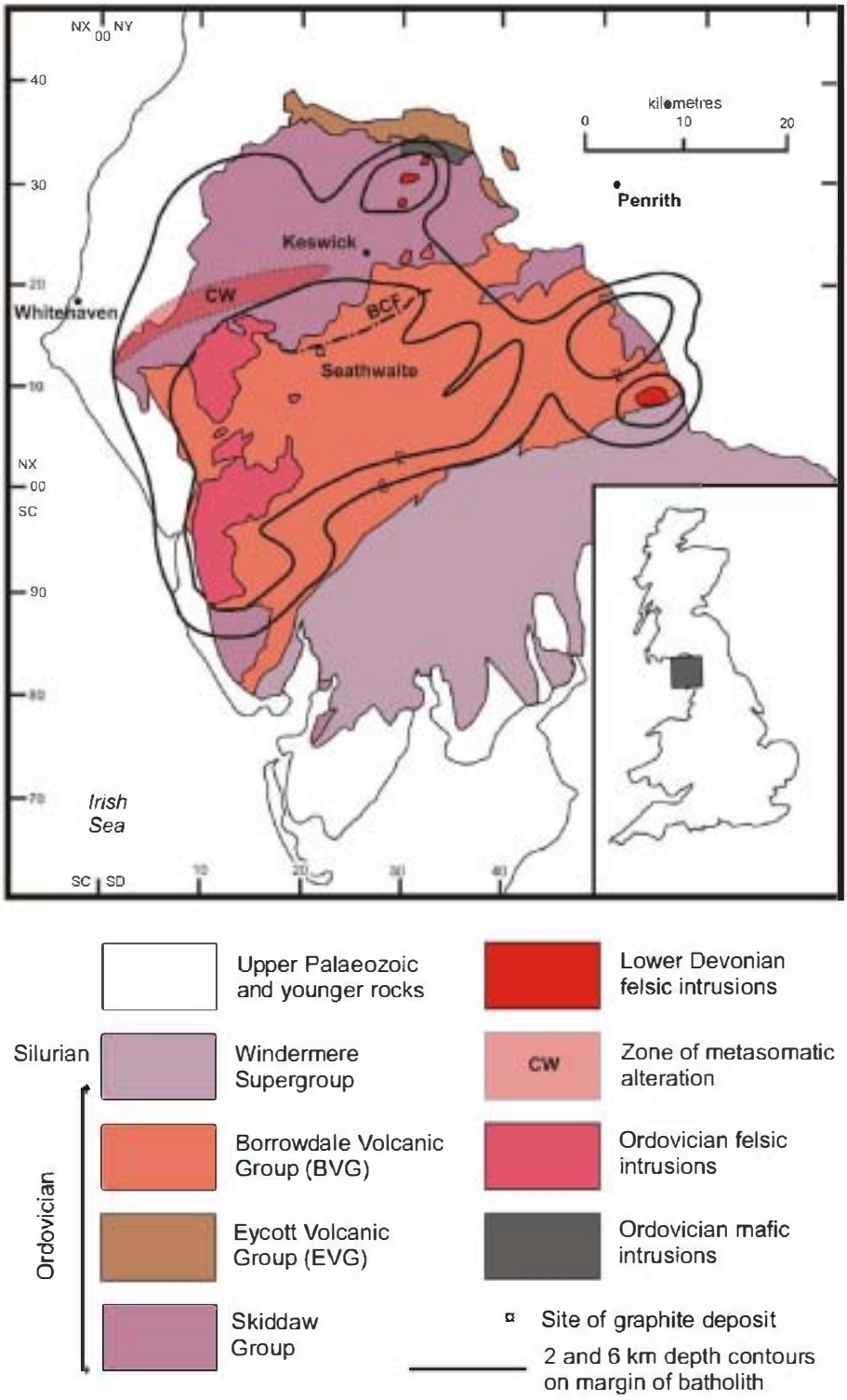

Fig. 1. Outline of the geology of the Lake District Lower Palaeozoic Inlier, UK. BCF, Burtness Comb Fault (Millward, 2002); CW, Crummock Water aureole (Cooper et al., 1988).

some samples from the spoil heaps were also collected. Samples of pelitic Skiddaw Group rocks were collected from three of its formations (Loweswater, Kirk Stile, and Buttermere formations). The three different formations sampled contain the greatest proportion of hemipelagic sediment, and therefore are thought likely to have the highest content of algal phytoplanktonic remains. The sample sites were also selected outside of known areas of hydrothermal

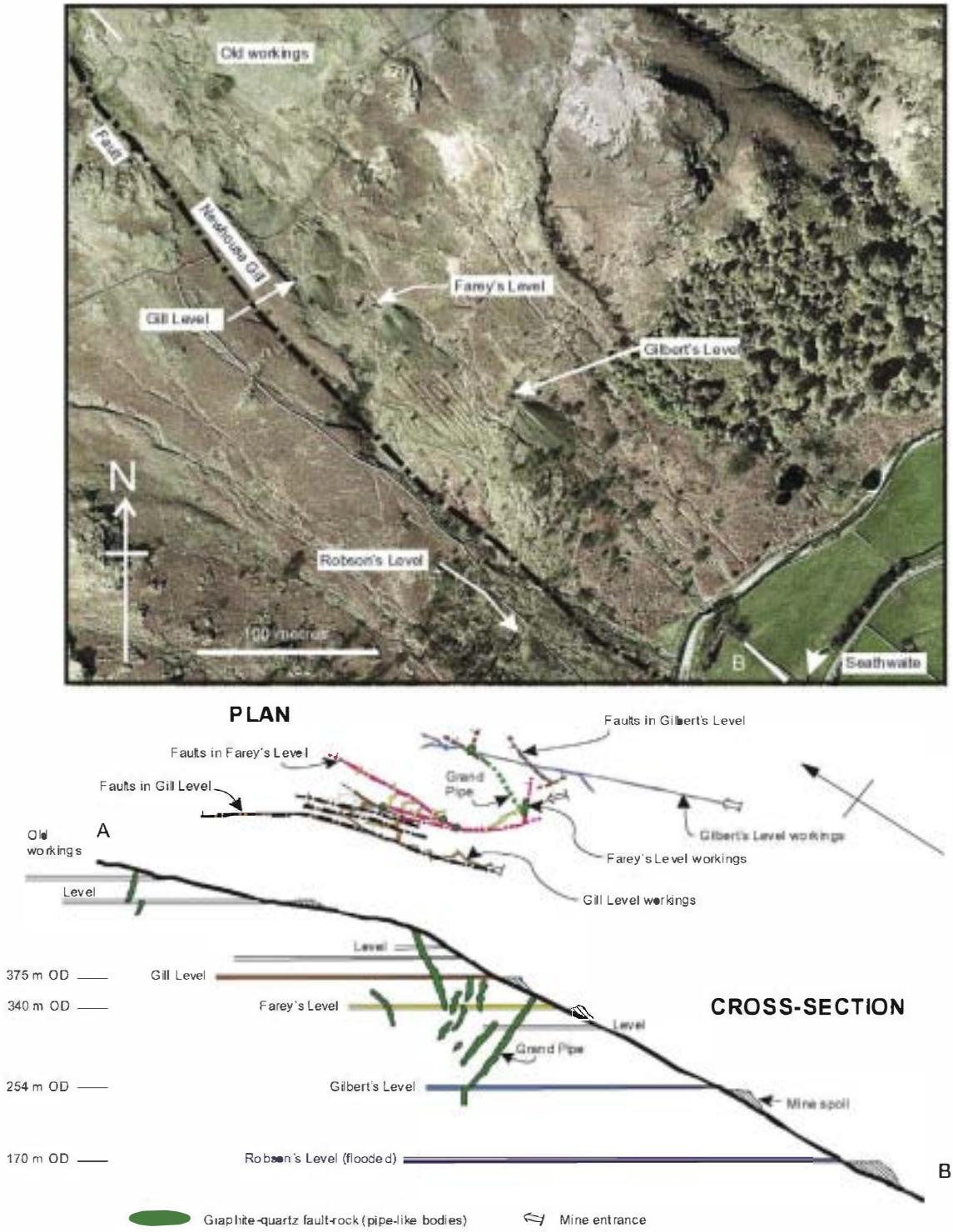

Fig. 2. Orthorectified aerial photograph, geological plan and cross-section of the Borrowdale graphite workings. Aerial photograph © UKP/Getmapping licence No. UKP2006/01. The cross-section 'AB' is a projection of some of the known workings onto a single NW–SE profile and is modified after Ward (1876). The plan shows the extent of some workings on the graphite veins on Gill, Farey's, and Gilbert's levels, explored as part of the current study. Level working plans from archives held by the British Geological Survey. Geological information on the plan from the current survey. Fault ticks indicate the downthrow side. The scale of the plan and cross-section is the same as the aerial photograph.

alteration/thermal metamorphic aureoles, such that these were only to have been affected by burial metamorphism.

Fluid inclusions were studied in quartz fragments associated with graphite in the mineralized bodies. Microthermo-

metric measurements were carried out at the Department of Crystallography and Mineralogy, Universidad Complutense, Madrid, on doubly polished sections, ~200 μm thick, using a Linkam THMS 600 heating–freezing stage, which is connected to a TMS92 programmable thermal control unit (temperature range between −190 and +600 °C). The following temperatures were measured: (1) final melting and homogenization of the carbonic CO_2–CH_4 phase in mixed aqueous-carbonic inclusions; $T_{h_{CAR}}$ (liq_{CAR} + vap = liq_{CAR}), respectively; (2) final melting temperature of ice in aqueous inclusions: $T_{m_{ice}}$ (ice + liq_{AQ} + vap = liq_{AQ} + vap); (3) clathrate melting: $T_{m_{CL}}$ (liq_{CAR} + liq_{AQ} + cla + vap = liq_{CAR} + liq_{AQ} + vap); (4) total homogenization temperatures of mixed aqueous-carbonic inclusions: $T_{h_{TOT}}$ (liq_{AQ} + liq_{CAR} = liq). Pure CO_2 and H_2O inclusions were used for calibration at the triple points (−56.6 and 0 °C). Measurements of $T_{m_{CAR}}$, $T_{m_{ice}}$, $T_{m_{CL}}$, and $T_{h_{CAR}}$ have an accuracy of ~0.5 °C.

Raman spectra of the carbonic species within the fluid inclusions were obtained using a Renishaw InVIA microspectrometer (ENS Paris) on the polished thin sections used for the petrographic study. We used a 514-nm Spectra Physics argon laser in circular polarization. The laser was focused on the sample by a DMLM Leica microscope with a 100× objective (Numerical aperture = 0.90), and the laser power at the sample surface was set around 1 mW. The Rayleigh diffusion was eliminated by edge filters, and the backscattered signal was finally dispersed using a 1800 lines-mm dispersive grating and analyzed by a Peltier cooled RENCAM CCD detector. Under these conditions the spatial resolution is ~1 μm and the spectral resolution is close to 1 cm^{-1}. For the study of fluid inclusions the laser beam was focused within the inclusion and the spectra were recorded from 1200 to 1550 cm^{-1} and from 2700 to 3100 cm^{-1} using an acquisition time of 5 s and 10 accumulations. These conditions yielded a good signal/noise ratio to reach high definition of the CO_2 and CH_4 Raman bands, respectively. The Raman parameters (peak position, band intensity, and band area) were determined with the computer program PeakFit 3.0 using a Voigt function. Nitrogen was not found in any of the studied inclusions. Quantitative relative proportions of carbonic species were calculated from equations proposed by Dubessy et al. (1989).

Bulk composition, density, and molar volume of the fluid inclusions (see Section 4.2 for the detailed description of fluid inclusion types) were calculated from microthermometric and Raman data with the computer programs BULK, version 01/03, and DENSITY, version 12/02 (Bakker, 1997, 2003; Bakker and Brown, 2003) using the Duan et al. (1992a,b) equation of state and considering NaCl as the only salt in solution. BULK was the preferred program for type V inclusions because $T_{h_{CAR}}$ was accurately measured in metastable absence of clathrate in all the studied inclusions. By contrast, clathrate was not visible in most of them, notably those having low percentage of aqueous liquid phase at 20 °C. Salinity for type V inclusions with known clathrate melting temperature ($T_{m_{CL}}$) was calculated with DENSITY. Isochores for the V inclusions with known salinity were calculated with the program ISOC 1.03 (Bakker, 2003) using the Bakker (1999) and Bowers and Helgeson (1983) equations of state. L2 inclusions did not show either observable V–L transitions in the gas phase or clathrate melting, and an average bulk composition was estimated with BULK assuming a low density for the CH_4-rich gas phase. Bulk composition and density could not be determined for L1 inclusions due to two reasons: the absence of CO_2 homogenization ($T_{h_{CAR}}$) and the low reliability of $T_{m_{CL}}$ reflecting the actual composition of the fluid (Murphy and Roberts, 1995).

Chemical compositions of minerals in the volcanic host rocks and within graphite nodules were analyzed by electron-microprobe (EMPA) using a JEOL Superprobe JXA 8900-M, under the following instrumental conditions: accelerating voltage of 15 kV, current of 20 nA, and beam diameter of 5 μm. Standards with similar compositions to the analyzed minerals were used (see Jarosewich et al., 1980, for details on the standard samples). Back-scattered electron (BSEM) images were recorded for the minerals analyzed.

XRD was performed on graphite samples from the deposit and also on Skiddaw Group metapelites. XRD data on graphite from the deposit has been previously reported (Luque et al., 2009). For the Skiddaw metapelites, after grinding and homogenization of the samples to <53 μm, random-orientated powders were examined on a Siemens Kristalloflex 810 diffractometer, using Cu K_α radiation at 30 kV and 40 mA, a step size of 0.03° (2θ), a slit system of 1°–1°–1°–0.15°, and time per step of 1 s (scan rate of 1.8° 2θ/min). In addition to the bulk mineralogy, the identification of clay minerals in the metapelites was carried out on orientated aggregates (OA) of the <2 μm fraction obtained by sedimentation onto glass slides from an aqueous suspension. For the identification of the clay minerals three types of OA were prepared: air dried, glycol-solvated, and heat treated at 550 °C. A slower scan rate (1.2° 2θ/min) was used between 2° and 13° 2θ in order to define peaks better. The full-width-half-maximum (FWHM) of the illite 10 Å peak (the so-called Kübler index, KI), was measured on the XRD patterns of the air-dried OA using the Diffrac Plus EVA 10.0 software. Our raw data were recalculated after calibration using reference polished slate slabs according to the procedure suggested by Kisch et al. (2004). The raw data can be transformed by the formula: $y = 1.0059x - 0.0493$. Therefore, the lower and upper limits of the anchizone are 0.38° and 0.21° Δ2θ, respectively.

Carbonaceous material in samples SK-1 and SK-2 from the Skiddaw Group was characterized by Raman microspectroscopy. Raman microspectroscopy was implemented to characterize the structural state of carbonaceous material in our samples and in order to obtain an estimate of the maximum temperature reached during metamorphism (RSCM, Raman Spectroscopy of Carbonaceous Material thermometry, Beyssac et al., 2002). Analytical conditions are described in detail in Beyssac et al. (2002, 2004).

The elemental carbon content of the Skiddaw metapelite samples was calculated using the total ion beam area (in units of amp-sec) generated from the isotope ratio mass spectrometry (IRMS) analysis. Each sample's total ion beam area (TBA) was compared with the TBA of the reference standard, in this case cane sugar (42.10 %C). The stan-

dard deviation of the data was less than 0.05 wt%. In addition, independent measurements of the carbon contents were carried out in a TOC-V CHS Shimadzu Total Organic Carbon (TOC) analyzer at the Faculty of Environmental Sciences (University of Castilla-La Mancha, Spain), equipped with a Shimadzu solid sample module SSM-5000A. Glucose was used as standard for calibration, and the precision of the measurements is within 1% of the determined amount of carbon. The analytical method consists of combustion and oxidation at a furnace temperature of 900 °C. Carrier gas was oxygen (99.9%), flowing at 500 mL/min. Elemental carbon analyses were done on powdered and homogenized samples of <53 and <25 μm.

Bulk stable carbon isotope analysis of graphite was performed at Geochron Laboratories (Massachussetts, USA). Samples were obtained from small holes excavated using a dentist's drill on unweathered surfaces of graphite nodules; although these powders contain silicate impurities, their graphite contents allowed for reproducible analyses. The analytical procedure was described in detail in a previous paper (Barrenechea et al., 1997).

Samples of Skiddaw Group metapelites were also analyzed at Iso-Analytical laboratories (Cheshire, UK) by EA-IRMS (elemental analyzer-isotope ratio mass spectrometry). Samples and references were weighed into tin capsules, sealed, and loaded into an auto-sampler on a Europa Scientific elemental analyzer. Samples were then dropped in sequence into a furnace held at 1000 °C and combusted in the presence of oxygen. The tin capsules flash combust, raising the temperature in the region of the sample to ~1700 °C. The combusted gases were swept in a helium stream over combustion catalyst (Cr_2O_3), copper oxide wires (to oxidize hydrocarbons), and silver wool to remove sulphur and halides. The resultant gases, N_2, NO_x, H_2O, O_2, and CO_2 were swept through a reduction stage of pure copper wires held at 600 °C. This removed any oxygen and converted NO_x species to N_2. A magnesium perchlorate chemical trap was used to remove water. Nitrogen and carbon dioxide were separated using a packed column gas chromatograph held at a constant temperature of 100 °C. The resultant carbon dioxide peak entered the ion source of the Europa Scientific 20-20 IRMS where it was ionized and accelerated. Gas species of different mass were separated in a magnetic field and then simultaneously measured using a Faraday cup collector array to measure the isotopomers of CO_2 at m/z 44, 45, and 46. The analysis proceeded in a batch process by which a reference was analyzed followed by a number of samples and then another reference. The reference material used for analysis was IAEA-CH-6 ($\delta^{13}C_{V\text{-}PDB} = -10.43‰$).

Four samples of pyrite-bearing andesite in which graphite nodules also appear were selected for sulphur isotope analysis to check for the source of sulphur. Calcite commonly overgrows the cubic pyrite crystals, so carbonate was removed from the igneous rock samples prior to analysis by acid digestion with 10% hydrochloric acid at room temperature for 12 h. Acid was removed by triple washing of the remaining sample material with de-ionized water prior to oven drying at 60 °C. Sample analysis was undertaken in duplicate by EA-IRMS at Iso-Analytical laboratories. Tin capsules containing reference or sample material plus vanadium pentoxide as oxidizing reagent were loaded into an auto-sampler, from where they were dropped, in sequence, into a furnace held at 1080 °C and combusted in the presence of oxygen. Tin capsules flash combust, raising the temperature in the region of the sample to ca. 1700 °C. The combusted gases are then swept in a helium stream over combustion catalysts (tungstic oxide/zirconium oxide) and through a reduction stage of high purity copper wires to produce SO_2, N_2, CO_2, and water. Water was removed using a Nafion™ membrane. Sulphur dioxide was resolved from N_2 and CO_2 on a packed GC column at a temperature of 32 °C. The resultant SO_2 peak entered the ion source of the IRMS where it was ionized and accelerated. Gas species of different mass were separated in a magnetic field then simultaneously measured on a Faraday cup universal collector array. Analysis was based on monitoring of m/z 48, 49 and 50 of SO^+ produced from SO_2 in the ion source. The reference material used during analysis of the samples was IA-R036 (barium sulphate, $\delta^{34}S_{V\text{-}CDT} = +20.74‰$). IA-R036, IA-R025 (barium sulphate, $\delta^{34}S_{V\text{-}CDT} = +8.53‰$)
+3.96‰) were used for calibration and correction of the ^{18}O contribution to the SO^+ ion beam.

Chlorite from two chlorite–graphite veins was analyzed for stable oxygen and hydrogen isotopes at the GNS Stable Isotopes Laboratory (New Zealand). In order to obtain chlorite concentrates, samples were crushed in a jaw-mill and ground further in a disc-mill. Then they were sieved to a 0.2–0.3 mm size. The resulting material was thoroughly washed and dried in a stove at 60 °C for 24 h. Chlorite was then concentrated with a Frantz laboratory isodynamic magnetic separator (model L-1). The purity of the chlorite concentrates was checked by XRD. Oxygen was extracted from chlorite for isotope analyses using a CO_2-laser and BrF_5 (Sharp, 1990). Oxygen isotope values are reported in the familiar $\delta^{18}O$ notation, relative to V-SMOW. Samples were normalized to the garnet standard UWG-2 using a value of +5.8‰
varied by less than 0.1‰. Samples and standards were heated overnight to 150 °C in a muffle furnace (to remove adsorbed moisture) prior to loading onto the vacuum extraction line. Blank runs were done to ensure that yields were less than 0.1 μmol oxygen. Oxygen yields of samples were recorded to ensure good oxygen yields and sample CO_2 gas was analyzed on a Geo20-20 mass spectrometer.

Hydrogen isotope values of chlorite were obtained on an Isoprime mass spectrometer coupled with a Hekatek high temperature (ca. 1600 °C) analyzer, configured for hydrogen isotope analyses. The results were normalized to IAEA CH-7 Polyethylene (−100.3‰)
(−66‰).
is better than 0.5‰

Differential thermal analysis (DTA) and thermogravimetric (TG) curves of graphite were simultaneously recorded using a Seiko TG/TDA 320U apparatus. For these analyses the samples (gently ground and sieved to <53 μm) were heated at 10 °C/min in the range 20–1000 °C, with a continuous air supply of 50 ml/min. Under these conditions complete graphite combustion is guaran-

teed (Crespo et al., 2006). Alumina was used as reference material.

4. RESULTS

4.1. The graphite deposit

The Borrowdale graphite deposit occupies about a 400 m length of a conjugate set of normal faults hading up to 45°. Strens (1965) recorded five faults striking 158–182° and three at 105°. Narrow veins and stringers filling the faults comprise massive graphite and chlorite along with quartz, but the richest deposits are developed at the intersections of the faults where there are steeply inclined pipe-like bodies up to 1 × 3 m in cross-section and from a few metres to over 100 m in length (Ward, 1876; Fig. 2). Graphite in the pipe-like bodies occurs as subspherical to ellipsoidal aggregates (nodules hereafter) and as irregular patches or small veins within altered andesite and dioritic host rocks (Fig. 3A). Nodules and patches may reach up to 10–15 cm in diameter or major length; their typical size is 1–2 cm, though nodules up to 1 m have been recorded (Ward, 1876). In places, graphite nodules are surrounded by greenish chloritic haloes (Fig. 3B). Rounded fragments of sandstone have been found in close association with the graphite nodules (Fig. 3C). In summary, graphite in the Borrowdale deposit occurs in three different contexts: (i) as nodular masses within the pipe-like bodies, (ii) along fault planes in the volcanic rocks, usually associated with chlorite, and (iii) as replacements (disseminations) within the igneous host rocks.

A great diversity of graphite morphologies within the Borrowdale deposit has been recognized (Barrenechea et al., 2009). Graphite in the nodules and patches from the pipes mainly occur as (1) flakes (the most abundant morphology in the deposit, >90%), (2) cryptocrystalline aggregates (mostly as colloform masses usually surrounded by flaky graphite), and (3) spherulites (5–40 μm in diameter, within laminar graphite). Composite nodules formed by cryptocrystalline graphite surrounded by flaky graphite have been found. Nodules and patches formed exclusively by flaky graphite frequently include radiating aggregates of elongate epidote crystals (Fig. 4A). The composition of the epidote is very homogeneous, corresponding to $Ca_2(Mn_{0.01}Mg_{0.01}Fe^{3+}_{0.75}Ti_{0.01}Al_{2.25})(Al_{0.02}Si_{2.98})O_{12}(OH)$ or to Ps_{25} if expressed as the pistacite content (Table 1). Chlorite, polycrystalline quartz, pyrite, chalcopyrite and minor sericite may also occur within the graphite nodules.

Graphite in chlorite–graphite veins also appears with flaky (predominantly) and spherulitic morphologies. The composition of chlorite in the veins is given in Table 1. Chemical analyses point to two different chlorite compositions that are intimately associated forming fan-shaped aggregates (Fig. 4B). The H and O isotopic data for chlorite from the veins fall within very narrow ranges, with average values of $\delta^{18}D_{V\text{-}SMOW} = -63.4‰$ respectively (Table 1). δD_{H_2O} values were calculated from the chlorite analyses using the fractionation relationship of Graham et al. (1987), and $\delta^{18}O_{H_2O}$ values were calculated by extrapolation of the fractionation data given by Cole and Ripley (1998).

The yellow-brown matrix within the mineralized pipe-like bodies comprises intensely altered wall rock and brecciated quartz. Also, both the andesite and dioritic wall rocks adjacent to the veins have been intensely hydrothermally altered to a propylitic assemblage containing quartz,

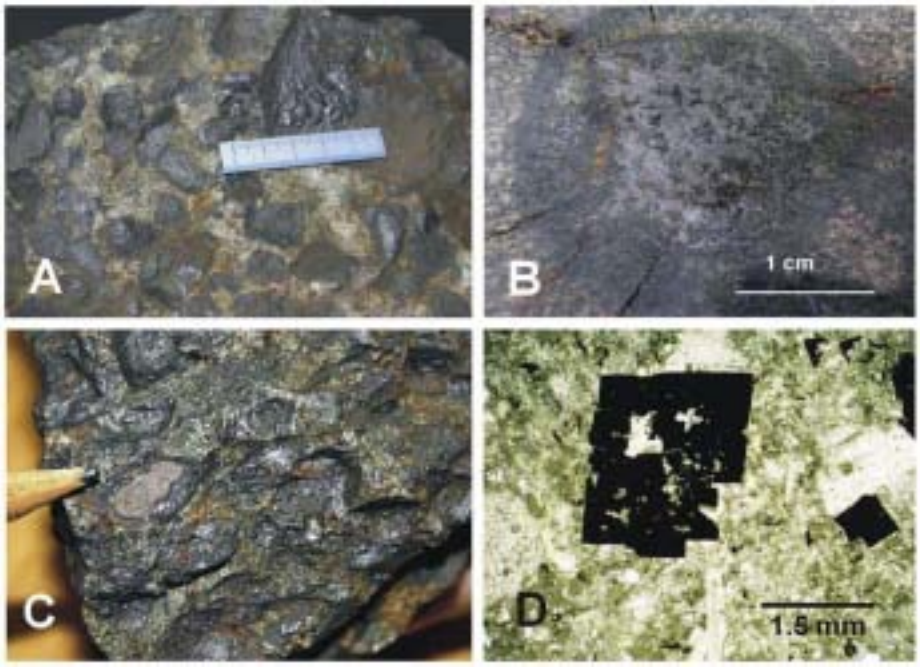

Fig. 3. (A) Hand specimen of altered diorite containing rounded nodules of graphite. (B) Chlorite alteration halo surrounding a graphite nodule within altered diorite. (C) Hand specimen showing graphite nodules and one untransformed xenolith of Skiddaw Group sandstone. (D) Transmitted light photomicrograph of subhedral pyrite crystals within altered andesite.

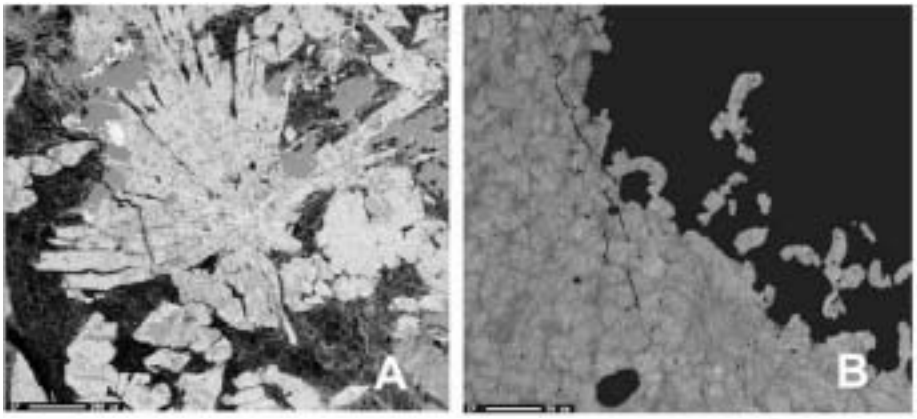

Fig. 4. Backscattered image (EPMA) of (A) radiating aggregate of epidote crystals within a graphite nodule, and (B) chlorite and graphite from a chlorite graphite vein. The black material in both images is graphite.

Table 1
Chemical and stable isotope composition of minerals from the Borrowdale deposit.

Element	Chlorite 1 (veins) ($n=10$)	Chlorite 2 (veins) ($n=8$)	Chlorite (andesite) ($n=9$)	Element	Epidote ($n=12$)
SiO_2	23.86 (0.36)	24.47 (0.27)	27.48 (0.61)	SiO_2	37.48 (0.46)
Al_2O_3	21.66 (0.38)	21.53 (0.25)	20.57 (0.72)	Al_2O_3	24.02 (0.65)
FeO	32.78 (0.57)	31.24 (0.42)	23.54 (1.31)	Fe_2O_3[a]	12.55 (1.10)
MnO	1.90 (0.14)	1.74 (0.08)	0.96 (0.17)	MnO	0.18 (0.08)
MgO	7.28 (0.26)	8.64 (0.43)	13.92 (1.92)	MgO	0.12 (0.07)
CaO	0.03 (0.01)	0.03 (0.01)	0.21 (0.09)	CaO	23.5 (0.84)
Na_2O	0.03 (0.02)	0.02 (0.01)	0.03 (0.02)	Na_2O	0.01 (0.01)
K_2O	0.02 (0.02)	0.01 (0)	0.03 (0.01)	K_2O	0.16 (0.09)
TiO_2	0.036 (0.02)	0.04 (0.01)	0.04 (0.02)	TiO_2	0.13 (0.06)
NiO	0.02 (0.01)	0.03 (0.02)	0.03 (0.02)	NiO	0.05 (0.03)
Cr_2O_3	0.02 (0.01)	0.02 (0.01)	0.23 (0.14)	Cr_2O_3	0.02 (0.01)
P_2O_5	0.01 (0.01)	0.02 (0.01)	0.12 (0.07)	P_2O_5	0.03 (0.02)
Total	87.63	87.74	87.14	Total	98.2
Si	5.30	5.37	5.79	Si	2.98
$Al^{(IV)}$	2.70	2.63	2.21	$Al^{(IV)}$	0.02
Ti	0.01	0.01	0.01	Ti	0.01
$Al^{(VI)}$	2.97	2.94	2.90	$Al^{(VI)}$	2.25
Fe^{2+}	6.09	5.73	4.15	Fe^{3+}	0.75
Mn	0.36	0.32	0.17	Mn	0.01
Mg	2.41	2.83	4.37	Mg	0.01
Ca	0.01	0.01	0.05	Ca	2.00
Na	0.01	0.01	0.01	Na	0.00
K	0.01	0.00	0.01	K	0.02
				Ps[b]	25.01
	$\delta^{18}O$ ($n=4$) = 2.5 (±0.01)‰				
	δD ($n=11$) = −63.4 (±0.4)‰				

n = number of analyses; standard deviation is given in brackets.
[a] Total Fe as Fe_2O_3.
[b] $Ps = 100(Fe^{3+}/Fe^{3+} + Al^{VI})$.

chlorite, sericite, and albite, along with some disseminated small aggregates of graphite and late calcite veinlets. Chlorite replaces the original ferromagnesian minerals, and sericite at least partially replaces the original plagioclase crystals. Chlorite compositions in the host rocks are more Mg-rich than those in the graphite–chlorite veins (Table 1). Graphite disseminations in the volcanic host rocks may occur as flakes, colloform aggregates, spherulites, and discs. Pyrite is also a common mineral in the andesite host rock, usually as subhedral to euhedral crystals (up to 2 mm long) which in places have been overgrown by small calcite or quartz crystals orientated perpendicular to the pyrite crystal faces (Fig. 3D). Sulphur isotope data of the pyrite range from $\delta^{34}S_{V\text{-}CDT} = 4.37$–$6.99$‰, ment with previously published results of pyrite in andesite rocks from the BVG in this area (Lowry et al., 1991). Additionally, a widespread hematization is observed close to the graphite–chlorite veins.

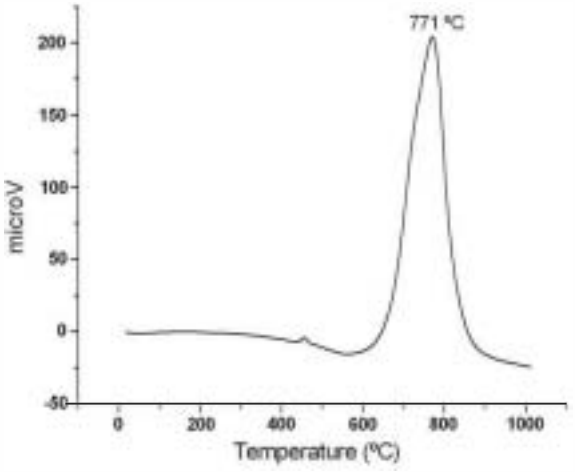

Fig. 5. DTA curve of graphite from the Borrowdale deposit, showing the temperature of the exothermic peak due to graphite combustion.

Graphite in the Borrowdale deposit displays very high crystallinity. XRD and Raman data (Luque et al., 2009) correspond to fully ordered hexagonal graphite with large crystallite sizes both along the stacking direction ($L_c = 1110$ Å) and along the basal plane ($L_a > 1000$ Å). Only colloform graphite grown over iron-bearing minerals (pyrite and silicates within the host rocks) has smaller in-plane crystallite sizes (L_a from 150 to 300 Å). In addition, thermal data indicate a high degree of crystallinity. The DTA curves show the exothermic maximum in the range from 747 to 771 °C (Fig. 5), comparable to other highly crystalline fluid-deposited graphites (Luque et al., 1998). Bulk carbon isotope data obtained from different parts of the nodules have $\delta^{13}C_{PDB}$ values ranging from −24.3 to −28.3‰.

geneous within a single nodule (Fig. 6), and show small variations from samples collected at different points of the

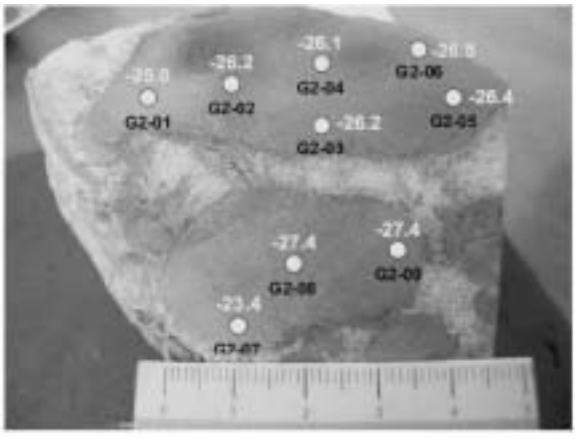

Fig. 6. Hand specimen with graphite nodules showing location of the points (white dots) analyzed for carbon isotope ratios. The figures in white correspond to the $\delta^{13}C$ values of each point. Note the homogeneity of the values within a given nodule (except for point G2-07) and the lack of any apparent isotopic zoning.

Table 2
Bulk stable carbon isotope ratios of selected graphite samples.

Sample	Location	$\delta^{13}C$ (‰)
P0-05	Grand Pipe	−26.9
P0-06	Grand Pipe	−25.8
G2−01	Gill's level	−25.0
G2-02	Gill's level	−26.2
G2-03	Gill's level	−26.2
G2-04	Gill's level	−26.1
G2-05	Gill's level	−26.4
G2-06	Gill's level	−26.5
G2-07	Gill's level	−23.4
G2-08	Gill's level	−27.4
G2-09	Gill's level	−27.4
G2-10	Gill's level	−26.5
G2-11	Gill's level	−27.1
G2-12	Gill's level	−26.6
G2-13	Gill's level	−26.6
G4	Gill's level	−27.1
G6	Gill's level	−26.3
GB3	Gilbert's level	−28.3
GB9	Gilbert's level	−28.3
P2-1	Grand Pipe	−26.3
F1-1	Farey's level	−26.4
F1-2	Farey's level	−26.3

P, samples from the Grand Pipe; G, samples from Gill's level; GB, samples from Gilbert's level; F, samples from Farey's level (chlorite graphite veins).

pipe-like bodies (Table 2). These results are in agreement with previously published bulk isotopic data for the Borrowdale graphite ($\delta^{13}C = -27.2$; Weis et al., 1981). However, bulk $\delta^{13}C$ values are slightly heavier than those reported for individual analyses of the most common graphite morphology (flakes) within the nodules (average $\delta^{13}C_{PDB} = -30.26$‰;

4.2. Fluid inclusion study

Fluid inclusions were studied in quartz fragments associated with the graphite nodules in the mineralized pipes (Fig. 7A). The angular shape of the fragments and their well distributed occurrence indicate that this quartz was brecciated, torn from its original location and transported upwards within the near vertical structures. Graphite nodules and patches commonly include quartz fragments and, less frequently, quartz encloses graphite crystals and aggregates (Barrenechea et al., 2009). Thus, the transport of quartz fragments along the pipes and graphite deposition were coeval. Therefore, fluid inclusions in the quartz fragments should have recorded the fluids that were circulating during this event. The quartz fragments show an internal polycrystalline texture with individual grains containing abundant inclusions along trails (Fig. 7B and C). These grains are occasionally bounded by quartz recrystallized during the brecciation process. The fluid inclusions trapped in growth surfaces of such recrystallized areas of the quartz grains have an unequivocal primary origin (Fig. 7C and D).

The fluid inclusions can be grouped as low-density vapour-rich inclusions (V), and more dense liquid-rich inclu-

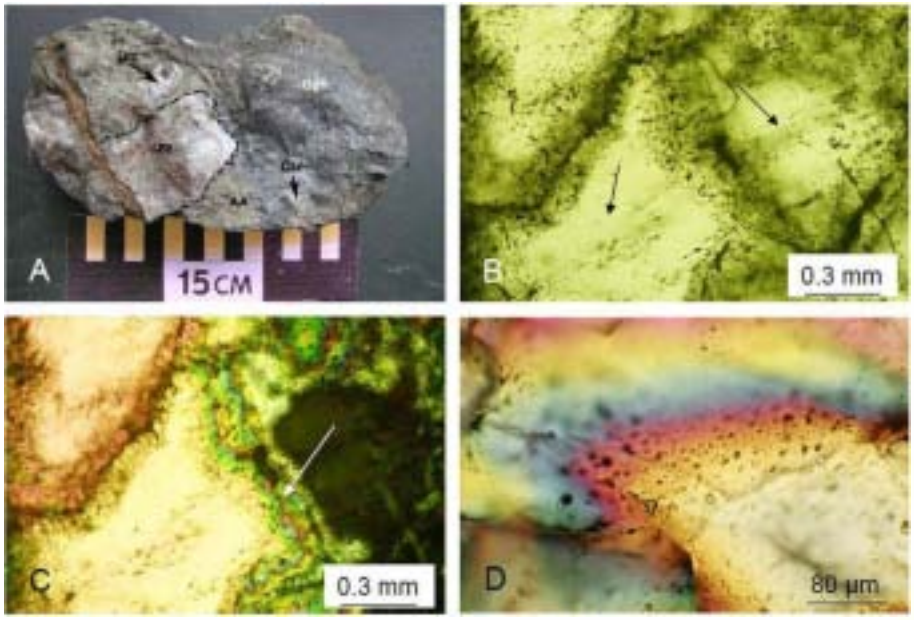

Fig. 7. (A) Hand specimen from the mineralized pipes in the Borrowdale deposit. The sample includes graphite (Gph) and an angular quartz fragment (Qtz) within an intensely altered andesite matrix (AA). Small quartz fragments are also embedded within the graphite mass. Photos (B–D) are transmitted light photomicrographs (B, one polar; C and D, crossed polars). (B and C) Polycrystalline internal texture of the quartz fragments, with trails of secondary inclusions within the core (marked by arrows in (B)). Dark appearance of the grain boundaries is due to the presence of abundant fluid inclusions. Recrystallization of quartz is observed in some boundaries (arrow in (C)). (D) Primary vapour-rich inclusions in bands of recrystallized quartz between quartz grains.

sions (L). A closer examination of the relative volume of the aqueous phase at room temperature, along with microthermometric and Raman data, has allowed the definition of four types of inclusions: V, VS, L1, and L2 (Fig. 8). Detailed Raman, microthermometric and calculated bulk compositional data are summarized in Table 3.

Type V corresponds to two-phase vapour-rich inclusions (Vv/Vt = 50–95%), made up of H_2O–CO_2–CH_4. These inclusions are relatively abundant and occur as primary inclusions in growth surfaces of recrystallized quartz (Fig. 7D) and, more frequently along trails within the clear cores of the quartz grains (Fig. 9A and B). In areas with a large number of inclusions, type V inclusions seem to be isolated within fields dominated by late L2 inclusions, which may have obliterated previous fluid inclusion assemblages. Raman data of the carbonic fraction in the type V inclusions indicate mixtures of CO_2–CH_4, with XCO_2 = 0.6–0.8. Their average bulk carbonic content ($XCO_2 + XCH_4$, mol fraction) varies from 0.8 in those inclusions with Vv/Vt > 0.9, in which the water phase is difficult to see at room temperature, to 0.33 in inclusions having Vv/Vt between 0.6 and 0.8. The XH_2O varies between 0.18 and 0.64, whereas the $XCO_2/(XCO_2 + XCH_4)$ ratio (#XCO_2 hereafter) is rather constant, having an average value of 0.69. Final melting and liquid homogenization of the CO_2–CH_4 phase ($n = 46$) occurs between −61.8 and

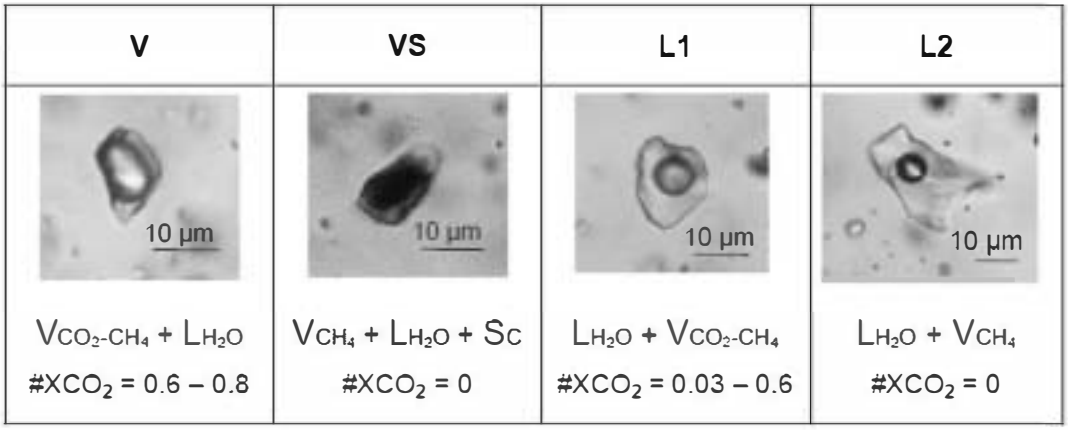

Fig. 8. Fluid inclusion types in quartz. V, vapour phase; L, liquid phase; S, solid phase; #$XCO_2 = XCO_2/(XCO_2 + XCH_4)$. See text for explanation of fluid inclusion features.

Table 3
Raman, microthermometric, and calculated compositional data of selected fluid inclusions from Borrowdale (for abbreviations, see text). Numbers in italics for the type V inclusions refer to those selected for the calculation of isochores in Fig. 12. The asterisk indicates those inclusions that underwent decrepitation before homogenization.

	Raman data		Microthermometric data				Bulk compositional data					
Vv/Vt	XCO_2	XCH_4	T_{hCAR}	T_{mICE}	T_{mCL}	T_{hTOT}	XH_2O	XCO_2	XCH_4	Salinity	Molar vol.	Density
Type V												
0.7 *(3)*	0.67	0.33	−1.9 L		+14.4	293 *	0.64	0.24	0.12	1.4	40.15	0.60
0.8	0.64	0.36	+0.5 L			332 V	0.53	0.30	0.17		49.37	0.52
0.5	0.75	0.25	+7.9 L			340 C	0.79	0.16	0.05		29.84	0.74
0.7 *(2)*	0.75	0.25	+3.8 L		+14.2	300 *	0.63	0.28	0.09	0.3	39.43	0.64
0.7 *(1)*	0.60	0.30	−8.1 L		+14.2	349 C	0.66	0.21	0.13	2.9	40.88	0.57
0.6	0.77	0.23	+2.7 L			275 *	0.72	0.22	0.06		33.68	0.70
0.7 *(4)*	0.75	0.25	+3.3 L		+14.2	321 V	0.63	0.28	0.09	0.4	39.39	0.64
0.6	0.81	0.19	+3.1 L			273 *	0.71	0.24	0.05		33.32	0.73
0.6	0.69	0.31	+4.1 L			338 V	0.73	0.19	0.08		34.40	0.66
0.9	0.77	0.23	+3.1 L			270 *	0.31	0.54	0.16		57.62	0.55
0.7	0.62	0.38	−9.9 L			267 *	0.65	0.22	0.13		40.46	0.58
0.95	0.68	0.32	−23.6 L				0.18	0.56	0.26		66.35	0.48
0.95	0.74	0.26	−13.6 L				0.17	0.61	0.22		64.20	0.52
0.95	0.72	0.28	−8.0 L				0.18	0.59	0.23		65.95	0.50
Type L1												
0.2	0.14	0.86		−7.0	10.5	276 L				8.1		
0.15	0.21	0.79		−6.1	10.5					7.3		
0.30	0.28	0.72		−6.7	9.0	321 L				7.2		
0.4	0.50	0.50		−7.2	10.5	372 L				5.7		
0.25	0.60	0.40		−5.5	11.1	220 *				5.0		
0.25	0.62	0.38		−6.0	10.5	283 *				5.6		
0.2	0.03	0.97		−4.2	16.0	342 L				4.4		
0.6	0.20	0.80		−7.1	9.5	348 L				4.0		
0.3	0.14	0.86		−5.9	10.5	290 L				6.3		
Type L2												
0.1		1		−5.1		195	0.98		0.02	8.0	19.07	0.97
0.1		1		−4.3		179	0.98		0.02	6.9	19.13	0.96
0.1		1		−3.7		183	0.98		0.02	6.0	19.18	0.96
0.1		1		−4.1		188	0.98		0.02	6.6	19.15	0.96

−57.1 °C, and in the range from −23.6 to +7.9 °C, respectively. Clathrate melting temperatures between +14.2 and +14.4 indicate salinities up to 3 wt% eq. NaCl. Total homogenization of the inclusions ranges from 295 to 340 °C (into vapour) and from 328 to 350 °C (critical behavior) indicating that the fluid was a vapour-like supercritical phase at the trapping conditions. Decrepitation prior to total homogenization at temperatures between 270 and 300 °C is relatively common. The average density of this fluid type is 0.6 g cm ^{3}.

Type VS inclusions consist of a large bubble containing pure CH_4 vapour plus highly crystalline graphite and a liquid H_2O phase (up to 15% vol.). These inclusions are very scarce (only three have been observed) and they occur closely associated with V and L1 inclusions (Fig. 9C and D).

Type L1 are two-phase liquid-rich H_2O–CO_2–CH_4-bearing inclusions (Vv/Vt = 25–40%) and they are notably less abundant than V and L2 inclusion types. They occur as isolated inclusions spatially associated with type V in the core of quartz grains (Fig. 9E and F), but they have never been observed along growth surfaces of recrystallized quartz. Furthermore, whereas trails containing only V inclusions are rather common (Fig. 9A), alignments formed only by L1 do not occur. These observations suggest that the L1 inclusions are slightly younger than V inclusions. Raman analysis indicate XCO_2 between 0.03 and 0.28 in most L1 inclusions ($n = 6$) and a further three inclusions had $XCO_2 = 0.5$–0.62 (Table 3). Although these three inclusions show #XCO_2 values close to type V inclusions, they were classified as L1 because the volume of the vapour phase is <0.5 and they do not show CO_2 homogenization. Microthermometry on 23 inclusions gave values of T_{mICE} in the interval −7.5 to −4.2 °C and T_{mCL} (measured by temperature cycling, Collins, 1979) between +9 and +16 °C. Bulk water content (mol fraction) is estimated to be high according to its volume fraction in the inclusions, with salinity ranging from 4 to 8 wt% eq. NaCl. Salinity values were derived from T_{mCL}. Total homogenization occurs between 276 and 372 °C into the liquid phase.

Type L2 are two-phase liquid-rich inclusions (Vv/Vt < 10%). They are very abundant and occur along trails (Fig. 9G) that occasionally cut across quartz grain boundaries, thus indicating that the inclusions are secondary in origin and post-date the type V and L1 fluid circulation. They also occur in groups of numerous inclusions close to the subgrain boundaries of the quartz (Figs. 7C and 9H). CH_4 is the only carbonic species in these inclusions, with an estimated average composition (mol fraction) of 0.98

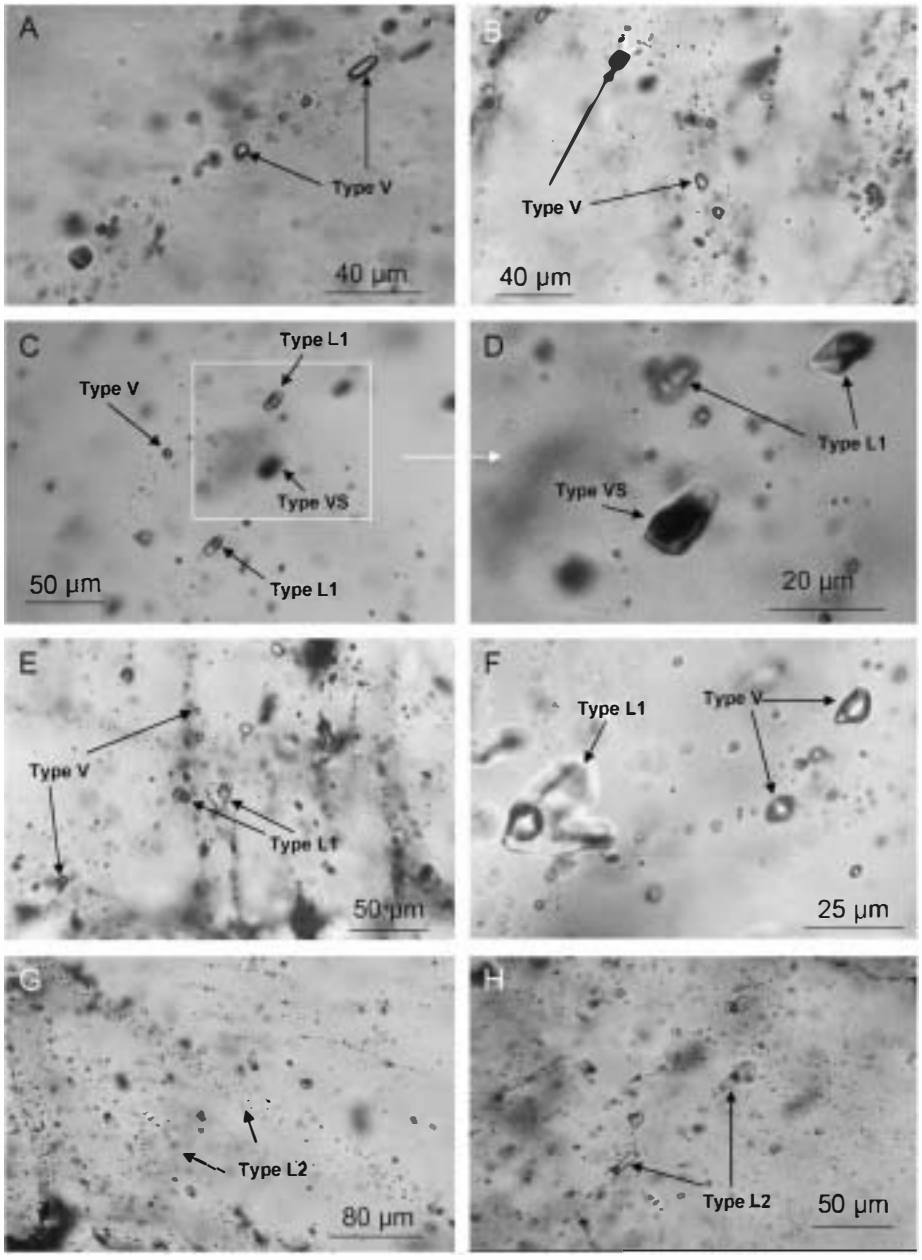

Fig. 9. Distribution of fluid inclusions in quartz (transmitted light photomicrographs, one polar). (A) Trail of secondary V inclusions, with no visible aqueous phase (Vv/Vt > 90%). (B) Type V inclusions with observable aqueous liquid. (C) VS inclusions spatially associated with V and L1 inclusions along trails. (D) Detail of photo (C). The black phase within the inclusion corresponds to highly crystalline graphite. (E and F) Isolated L1 inclusions, close to V inclusions trails. (G) Late L2 inclusion trails within the core of the quartz grains. (H) L2 inclusions in dark areas of the quartz close to grain boundaries (see Fig. 7B and C).

H_2O and 0.02 CH_4. Melting of ice occurs in the range −6 to −2.8 °C indicating salinities between 4.7 and 9.2 wt% NaCl. The total homogenization of the L2 inclusions ($n = 48$) occurs between 160 and 205 °C, with a maximum in the interval 180–195 °C ($n = 25$; Table 3).

4.3. Skiddaw Group metapelites

Samples from the Loweswater (SK-1), Kirk Stile (SK-2), and Buttermere formations (SK-3) within the Skiddaw Group show a well developed cleavage fabric. The mineral assemblages of these rocks consist of illite and chlorite, with subordinate amounts of quartz and trace amounts of K-feldspar. Both compositional and grain size banding are present with alternating light coloured bands composed mainly of very small particles of illite and quartz, and dark coloured bands consisting mainly of larger chlorite crystals and iron oxide. Small particles of carbonaceous matter also occur in both light and dark bands. Illite crystallinity (KI, raw values) ranges from 0.24° (Δ2θ) for samples SK-1

Table 4
Replicate stable carbon isotope analyses of Skiddaw metapelites.

Sample	δ^{13}Cv-PDB (‰)	
SK-1-1 (<53 μm)	−28.41	−28.34
SK-1-2 (<53 μm)	−27.78	−27.85
SK-1-3 (<25 μm)	−24.35	−24.38
SK-2-1 (<53 μm)	−29.86	−30.07
SK-2-2 (<53 μm)	−30.12	−30.09
SK-2-3 (<25 μm)	−28.14	−28.05
SK-3-1 (<53 μm)	−27.27	−27.38
SK-3-2 (<53 μm)	−27.41	−27.35
SK-3-3 (<25 μm)	−23.57	−23.41

and SK-2, to 0.37‰ ($\Delta 2\theta$) for sample SK-3. After calibration upon polished slate slabs (Kisch et al., 2004), these data are compatible with metamorphism at anchizonal to epizonal conditions, as previously suggested by Fortey (1989), Fortey et al. (1993) and Merriman (2006) for the whole Skiddaw Group.

The Raman study of carbonaceous material (CM) within the Skiddaw metapelites allowed the recognition of two main phases: a disordered pool and a highly graphitic one. The former is most abundant and corresponds texturally to organic matter transformed in situ during metamorphism, whereas the latter pool corresponds to detrital graphite (see Galy et al., 2008, for more details). Detrital particles are generally smaller than in situ CM but it is hard to define a size for in situ CM as it is generally texturally a continuous network. The spectra obtained for the in situ CM correspond to a maximum metamorphic temperature of 350 °C in both samples, with a standard error of less than ±5 °C and a calibration attached accuracy of ±50 °C (Beyssac et al., 2002), a very conservative estimate (cf. Beyssac et al., 2004).

Total organic carbon analyses in the studied Skiddaw Group samples reveal contents in the range from 0.31% to 0.86% for the <25 μm samples. The values presented here compare to the range of 0.039–0.59% determined on a small number of typical Skiddaw Group rocks reported by Cooper et al. (1988) and Bebout et al. (1999). It is worth noting that samples ground to <53 μm show significantly lower carbon contents (0.19–0.36%). This variation in the carbon content depending on the particle size is accompanied by a shift towards heavier δ^{13}C values (Table 4). These δ^{13}C values are within the range reported by Bebout et al. (1999) from bulk samples.

5. DISCUSSION

The Borrowdale deposit is a unique example of a large volume of highly crystalline, fluid-deposited graphite emplaced in a subvolcanic environment. Such an association requires the coincidence of a number of special features in its formation, as discussed below.

The isotope composition of the fluid calculated from the chlorite data in the chlorite–graphite veins (Fig. 10) supports the mixing of a magmatic fluid with a probable component of surface-derived fluid (meteoric water), which is quite common in subduction-related volcanic environments

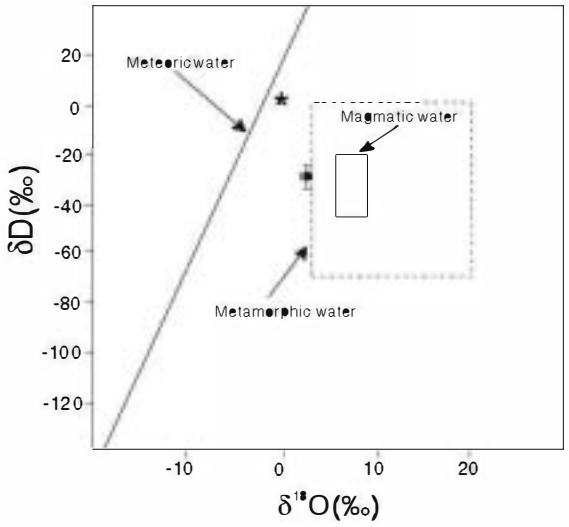

Fig. 10. Calculated fluid isotope compositions for the Borrowdale graphite deposit in relation to reference waters. The δD_{H_2O} and $\delta^{18}O_{H_2O}$ values calculated from chlorite. The arms of the cross depict the uncertainty of fractionation factors at the estimated temperature (400 °C) and the range of the isotopic values for chlorite (Table 1). Metamorphic water box from Sheppard (1986), magmatic water box from Hedenquist and Lowenstern (1994). The asterisk marks the composition of the reference SMOW water.

(Henley and Hedenquist, 1986; Hedenquist and Aoki, 1991; Hedenquist et al., 1994; Giggenbach, 1996; Giggenbach et al., 2003). The mineralization has an important tectonic control, with graphite occurring within near-vertical pipe-like bodies developed at the intersection of conjugate normal fractures which are also mineralized. These types of structure, especially the breccia pipes, imply an overpressured, fluid-rich regime which favoured the transport of andesitic and dioritic rocks and/or melts upwards and eventually resulted in the precipitation of huge amounts of graphite from such fluids. This fluid phase was recorded mostly as secondary inclusions in quartz xenoliths transported within the pipes.

5.1. Origin of carbon in the mineralizing fluids

The origin of carbon in C–O–H fluids can be recognized from the stable carbon isotope signatures of the precipitated graphite. The light isotopic signatures of both bulk graphite and of each of the different graphite morphologies from the Borrowdale deposit suggest that the carbon was derived from a biogenic source (Weis et al., 1981; Barrenechea et al., 2009).

There is geological and geochemical evidence of assimilation of Skiddaw Group metapelites by the volcanic host rocks (Fitton, 1972; Lowry et al., 1991; McConnell et al., 2002). These metapelitic rocks contain significant amounts of carbonaceous matter and they can be therefore regarded as the most probable source for carbon in the hydrothermal fluids responsible for the Borrowdale graphite deposit.

The bulk carbon isotopic analyses of Skiddaw metapelites yielded light δ^{13}C values within the typical range for biogenic carbonaceous matter. However, differences of 2–

4‰ have been observed between the different particle size fractions studied. The <25 μm-fractions of the three samples studied in this paper (Table 4) show heavier isotopic ratios than their respective coarser fractions (<53 μm). This can be attributed to isotopic differences corresponding to various organic precursors, as frequently recognized in low-grade metamorphic samples (Grew, 1974; Okuyama-Kusunose and Itaya, 1987; Kribek et al., 1994), or to a larger release of isotopically light methane from the smaller particles thus leaving a heavier residue of graphitized carbonaceous matter (Wada et al., 1994). Alternatively, the presence of carbonaceous particles with heterogeneous graphitizing degrees in low-grade metamorphic rocks can be ascribed to the co-existence with detrital graphite (e.g. Buseck and Huang, 1985; Wada et al., 1994; Beyssac et al., 2003; Crespo et al., 2004; Rantitsch et al., 2004; Galy et al., 2008; Judik et al., 2008). For the Skiddaw metapelites, the detrital contribution is favoured by the textural and Raman data.

Considering the stable carbon isotope ratios for the dominant carbonaceous material within the Skiddaw metapelites (the largest particles, <53 μm, graphitized in situ), the average $\delta^{13}C$ value is close to −28.5‰. The assimilation at high temperature of such carbonaceous matter by the andesite magma produced isotopically heavier CO_2. The fractionation between C and CO_2 at temperatures of about 1100 °C (the typical solidus temperature of andesite magmas) is $\alpha = 5.5$‰ (Scheele and Hoefs, 1992). Thus, the isotopic signature of the CO_2 formed through assimilation of carbon from the Skiddaw metapelites would be −23‰. This can be considered the initial value from which the isotopic signatures of graphite in the deposit were derived, as will be explained below.

5.2. Evolution of the fluids and conditions of graphite precipitation

The fluid inclusion types in quartz associated with graphite in the Borrowdale deposit reveal the evolution of the carbon-bearing fluids involved in the mineralizing process. The relative chronology of the fluid inclusions has been estimated from the petrographic analysis and the timing of fluid circulation can be established as follows: V → L1 → L2. The VS inclusions record a singular situation, located in time between the fluids represented by the V and L1 fluid inclusions, as will be discussed later. The compositional trend of the fluid inclusion assemblages shows an overall fluid evolution characterized by: (1) depletion in the carbonic species due to graphite precipitation, and (2) progressive decrease in the $\#XCO_2$ from the early V fluid to the late L2 fluid which contains only minor CH_4 and no CO_2 (Fig. 11).

The total homogenization temperatures of V and L1 within similar ranges (295–350 °C – into the vapour phase or critical, and 276–370 °C – into the liquid phase, respectively) suggest that these inclusions could be derived from a boiling process. However, these two groups of inclusions do not fulfil the necessary requirements of the V and the L fractions of a boiling fluid (Ramboz et al., 1982; Roedder, 1984) because (1) they were not trapped contemporaneously, and (2) $\#XCO_2$ is higher in V inclusions than in the L1-type. The latter point is contrary to the expected volatile fractionation between liquid and vapour produced during unmixing of aqueous-carbonic fluids, in which the vapour fraction would be enriched in the more volatile component, namely CH_4. Therefore, the petrographic and compositional data point to the conclusion that V and L1 inclusions likely represent the sequential trapping of different fluids.

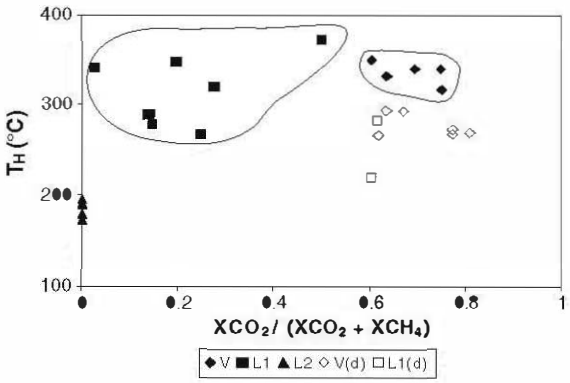

Fig. 11. $\#XCO_2 = XCO_2/(XCO_2 + XCH_4)$ vs homogenization temperature (T_H) for the different types of fluid inclusions. Note the decrease in $\#XCO_2$ from the earliest fluid (V) to L1 and, finally, to the latest one (L2). (d): Inclusions with decrepitation before total homogenization.

According to the proposed chronology, the type V, vapour-rich fluid represents the fluid circulating at the earliest stages of the process. Therefore, the V fluid should be the initial fluid from which graphite started to precipitate. The VS inclusions, containing highly crystalline graphite + CH_4 + H_2O, and always occurring closely associated with V inclusions, likely represent the massive precipitation of graphite from the V fluid in the deposit. Many authors (e.g. Kreulen, 1987; Van den Kerkhof et al., 1991) have pointed out that the mixtures of CO_2 and CH_4 within fluid inclusions are not stable and should follow the reaction $CO_2 + CH_4 \rightarrow 2C + 2H_2O$ precipitating graphite until one of the two components is totally consumed. The VS inclusions are rather uncommon, and most of the V inclusions show a narrow range of $\#XCO_2$ and lack of graphite crystals, thus indicating that the V fluid remained unchanged and metastable within the inclusions. This is probably related to the difficulty of graphite nucleation in the absence of graphite seeds within the inclusion cavities. L1 inclusions, trapped after the V inclusions, likely represent the fluid compositional change during graphite precipitation. The latest stage of fluid circulation is represented by L2 inclusions, occurring once graphite precipitation had ceased.

Chemical reactions and P–T–fO_2 conditions of graphite precipitation have been inferred from mineral assemblage, fluid composition, and isotopic data.

Graphite nodules and patches within the pipes frequently include chlorite and radiating aggregates of elongate epidote crystals. Whereas chlorite is widespread in the pipes, epidote is restricted to nodules exclusively composed of flaky graphite and shows a quite constant compo-

sition of Ps_{25}, indicating an oxygen fugacity corresponding to the FMQ (Liou, 1993). Chlorite is also associated with both graphite spherulites and flaky graphite within the graphite–chlorite veins (Barrenechea et al., 2009). The andesite and dioritic wall rocks were intensely hydrothermally altered to an assemblage containing quartz, chlorite, albite, and sericite. This assemblage is overprinted by late cross-cutting calcite veinlets and hematitization of wall-rocks. The features of the earlier mineral assemblage are indicative of an intense propylitic alteration, and provide evidence that graphite precipitated during this hydrothermal event. Suitable *PT* conditions for the beginning of graphite mineralization in the Borrowdale deposit have been estimated by Luque et al. (2009). Thermodynamic calculations carried out in this previous work show that carbon-saturated fluids with $\#XCO_2$ of 0.69 (type V fluid) and at fO_2 corresponding to the FMQ buffer are stable at temperatures of ~500 °C for a pressure of 2–3 kbar. This pressure interval was considered the most likely, as it is compatible with an emplacement of the graphite deposit in a subvolcanic setting (Millward, 2004). The isochores calculated for selected V inclusions in this study are consistent with the estimated *PT* conditions and constrain the beginning of graphite precipitation to a pressure close to 2 kbar (Fig. 12).

The composition of the V fluid at $T = 500$ °C and $P = 2$ kbar plots in the fluid + graphite field of the C–O–H diagram (Luque et al., 2009), indicating that the fluid was saturated in graphite at the time of trapping. Evidence of graphite morphologies corresponding to high supersaturation conditions in the Borrowdale deposit has been presented in a previous paper (Barrenechea et al., 2009). These morphologies, namely spherulites and cryptocrystalline colloform aggregates, represent the earliest stages of

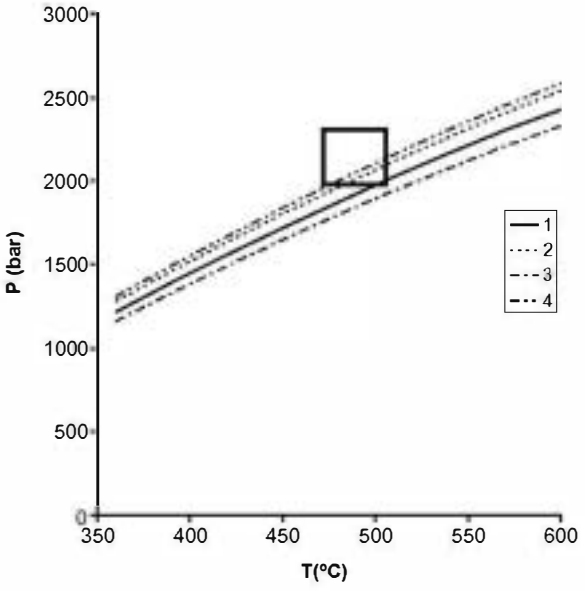

Fig. 12. *PT* diagram showing isochores for selected V-type fluid inclusions. The box indicates the inferred *PT* conditions for the beginning of graphite deposition (Luque et al., 2009). Numbers in the legend refers to the selected fluid inclusions (see Table 3).

graphite deposition, followed by flaky graphite as supersaturation decreased. The main stage of graphite precipitation (flaky graphite in nodules and patches within the pipes) should occur at temperatures lower than 500 °C considering the stability of the propylitic assemblage related to the mineralization. The stability of this assemblage has been checked using thermodynamic calculations in a phase diagram projection for the system C–O–H–FeO–MgO–Al_2O_3–Na_2O–CaO assuming equilibrium with graphite (VERTEX program; Connolly, 1990). The stability of ab + chl + ep + sericite(+qtz) is limited by ep + ab + sericite = chl + Kf + plag, which has a more or less constant *P–T* slope and occurs at ~400 °C at 2 kbar and ~500 °C at 7 kbar. Thermodynamic calculations therefore place the upper limit of temperature for the main stage of graphite precipitation (flaky graphite) at ~400 °C, that took place after an earlier stage (spherulites and cryptocrystalline colloform aggregates) initiated at higher temperature (~500 °C).

The main event of graphite mineralization must have occurred during a short period of time as supported by geological evidence, namely the pipe-like geometry of the main part of the deposit. Mine plans in the British Geological Survey archive show the presence of at least 12 pipe-like bodies that had been worked within the mine complex. The brecciated, mineralized pipe-like bodies, containing sporadic clasts of Skiddaw Group lithologies, suggest rapid transport of overpressured fluids upwards, similar to diatreme-like bodies. The homogeneous carbon isotopic signature both at the microscale (Barrenechea et al., 2009) and at the scale of each single nodule is also in agreement with such an interpretation. The isotopic signature of fluid-precipitated graphite is strongly dependent on (1) temperature, (2) bulk chemical composition of the fluid, and (3) oxygen fugacity (Duke and Rumble, 1986; Rumble et al., 1986; Luque et al., 1998; Farquhar et al., 1999). Any important change in one (or more) of these parameters implies relatively large isotopic variations. Thus, the existence of marked isotopic zoning is a common feature in fluid-deposited graphite at slow cooling rates (Luque et al., 1998; Binu-Lal et al., 2002; Santosh et al., 2003). For instance, Duke and Rumble (1986) showed that at $T = 600$ °C and $P = 3$ kbar, for compositions close to the water maximum of the C–O–H system, a variation of 0.4 log units fO_2 causes an isotopic shift of 5.1‰ in the graphite deposited. Similarly, for CO_2-rich aqueous fluids, a small variation from $XH_2O = 0.84$ to $XH_2O = 0.79$ leads to an isotopic shift of 4.6‰

at the above *PT* conditions and at those estimated for the Borrowdale deposit, similar quantitative variations could be expected. However, the isotopic signatures among the different graphite morphologies do not differ by more than 3‰

pic heterogeneities (usually less than 1.5‰) are observed in samples taken from a given nodule (Fig. 7, Table 3). All these observations allow us to infer that graphite deposition within the pipes occurred very rapidly from a C–O–H fluid and under more or less constant fO_2.

The graphite precipitation reactions and the related change in fluid compositions can be thermodynamically

modelled in the C–O–H system of which the calculation procedure is described in detail by French (1966) and Ohmoto and Kerrick (1977). The exact fluid composition can be calculated for a carbon saturated fluid if the fO_2 for the system is known. Thermodynamic data for the calculations were taken from Holland and Powell (1998) and fugacity coefficients were calculated using the data from Shi and Saxena (1992) assuming ideal mixing. The fO_2 is given relative to the fayalite–magnetite–quartz buffer (FMQ), using the equation from Ohmoto and Kerrick (1977).

Fluid compositional changes as a result of graphite precipitation can be visualized in a C–O–H ternary diagram (Fig. 13A). Oxidized fluids dominantly comprise H_2O and CO_2 whereas a reduced fluid consists of H_2O, CH_4, and small amounts of H_2. Fluids in the grey field are supersaturated in carbon and will precipitate graphite until it reaches an equilibrium fluid composition situated on the carbon saturation surface (Fig. 13A).

Among the reactions involving CO_2 and CH_4 from which graphite can precipitate from a C–O–H fluid we can consider the following (Ohmoto and Kerrick, 1977; Frost, 1979): (1) $CO_2 + CH_4 \rightarrow 2C + 2H_2O$, (2) $CO_2 \rightarrow C + O_2$, and (3) $CH_4 + O_2 \rightarrow C + 2H_2O$. The graphite precipitation is caused by carbon supersaturation of the fluid as a result of both cooling from 500 to 400 °C and withdrawal of H_2O from the fluid phase as a result of hydration reactions. Based on the isotope signature of graphite, the graphite forming reactions must all have taken place at constant fO_2 conditions. Early chlorite formation occurs during cooling from 500 to 400 °C, with consequent decrease in the mole fraction of H_2O of the fluid phase (trajectory 1 in Fig. 13B). This process proceeded until the fluid

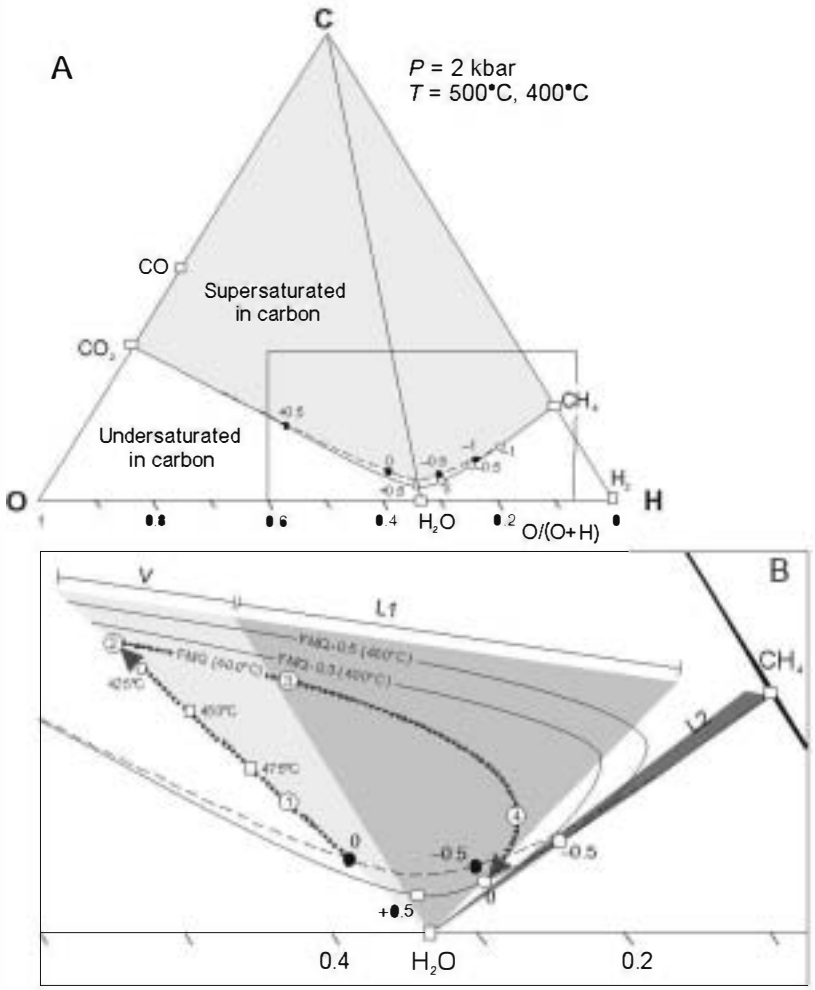

Fig. 13. (A) C–O–H fluid system at 2 kbar and 400, 500 °C showing carbon saturated fluid compositions as a function of the fluid fO_2 referred to as the carbon saturation surface (solid line: 500 °C, dashed line: 400 °C). Circles indicate fluid fO_2 in $\log_{10}$ units relative to FMQ (open circles: 500 °C, solid circles: 400 °C). The diagram was calculated using an updated version of the Excel spreadsheet COH (Huizenga, 2005). (B) Enlargement of the inset in (A). Indicated are iso-oxygen fugacity lines calculated at 400 °C. Fluid compositional variations during graphite precipitation are indicated with the grey dashed arrows. Trajectory 1 shows the H_2O depletion of a carbon saturated fluid due to hydration reactions during cooling until it reaches point 2. Trajectory 3 corresponds to the precipitation of graphite as result of the reduction of CO_2 while fO_2 remains at FMQ. During the final stage of graphite precipitation (trajectory 4), the dominant graphite precipitation reaction changes and becomes the oxidation of CH_4. Shaded areas: compositional fields of the different inclusion types (V, L1, and L2) based on $\#XCO_2$.

reached the temperature of 400 °C (point 2 in Fig. 13B). During this process the fluid fO_2 is controlled by the amount of H_2O withdrawal from the fluid phase (decreasing effect). However, the FMQ buffer will also decrease with decreasing temperature so the fluid fO_2 relative to FMQ may remain constant if the H_2O withdrawal and cooling are in pace. The cooling trend in order to keep the fluid fO_2 balanced at FMQ is indicated in Fig. 13B. The fluid fO_2 will decrease if the cooling lags behind the H_2O withdrawal. In that case the fluid fO_2 will decrease and re-equilibrate to its initial value of FMQ by the reaction $CO_2 + CH_4 = 2C + 2H_2O$. That this reaction did take place is shown by the presence of small graphite spherulites intergrown with chlorite in the andesite wall rock (Barrenechea et al., 2009, their Fig. 3a). This reaction results in an increase of $\#CO_2$ to become greater than 0.8 in the fluid phase. However, the absence of V-type fluid inclusions with a $\#CO_2 > 0.8$ implies that the above reaction only played a minor role. This contention is further supported by the composition of the graphite-bearing VS inclusions, which contains only CH_4, with no CO_2, thus suggesting that the main reaction of graphite precipitation from the V fluid could not be $CO_2 + CH_4 \rightarrow 2C + 2H_2O$ as it would result in the total consumption of CH_4.

From point 2 onwards, the fluid precipitated graphite at a constant temperature of ~400 °C during which the fluid composition changed along the FMQ iso-fugacity line. The dominant reaction during this process is $CO_2 = C + O_2$ (trajectory 3 in Fig. 13B). During this stage the mole fraction of CO_2 decreased and that of H_2O increased. The decrease in the mole fraction of CO_2 resulted in the crystallization of epidote as is demonstrated by the close relationship between epidote and flaky graphite within the pipes. Epidote is not stable for $XCO_2 > 0.2$ (Ferry and Burt, 1982; Liou, 1993) and the type V fluid contains an average bulk XCO_2 of 0.24. Therefore, epidote crystallization was likely triggered by the consumption of CO_2 in the graphite precipitation reaction. The reduction of CO_2 proceeded until the iso-fugacity line curved towards the O–H binary and the reaction $CH_4 + O_2 = C + 2H_2O$ became the dominant one. Graphite precipitation stopped when the fluid composition reached the carbon saturation surface. The FMQ iso-fugacity line crosses first the V and then the L1 compositional fields, explaining the formation of the V inclusions followed by the L1 inclusions (Fig. 13B). The final stage, would involve the formation of H_2O–CH_4 fluids (L2 fluid inclusions) after the fluid composition crossed the boundary of the carbon saturated field.

Local heterogeneities probably occurred in the relative contribution of the reactions proposed above to the graphite precipitation process. These changes are recorded in the isotopic signature of the precipitated graphite. Considering the isotopic signature of the assimilated carbon by the andesite magma ($\delta^{13}C = -23$‰) and the fractionation factor for CO_2–C of 10.5‰
ture estimated for the beginning of graphite precipitation (~500 °C; Luque et al., 2009), graphite deposited from the initial CO_2-rich fluid should have an isotopic signature close to −33.5‰
pic data for the earliest morphology crystallizing in the pipe-like bodies (i.e. colloform graphite with $\delta^{13}C = -33.7$‰;
pic variation among the different graphite morphologies and with respect to the bulk analysis of graphite nodules could be attributed to the evolution of the mineralizing C–O–H fluid. Thus, the local changes in the relative contributions of the graphite precipitation reactions would result in the observed isotopic heterogeneities, because such reactions influenced not only the relative amounts of carbon species in the fluid but also the XH_2O (Fig. 14). Fluids pro-

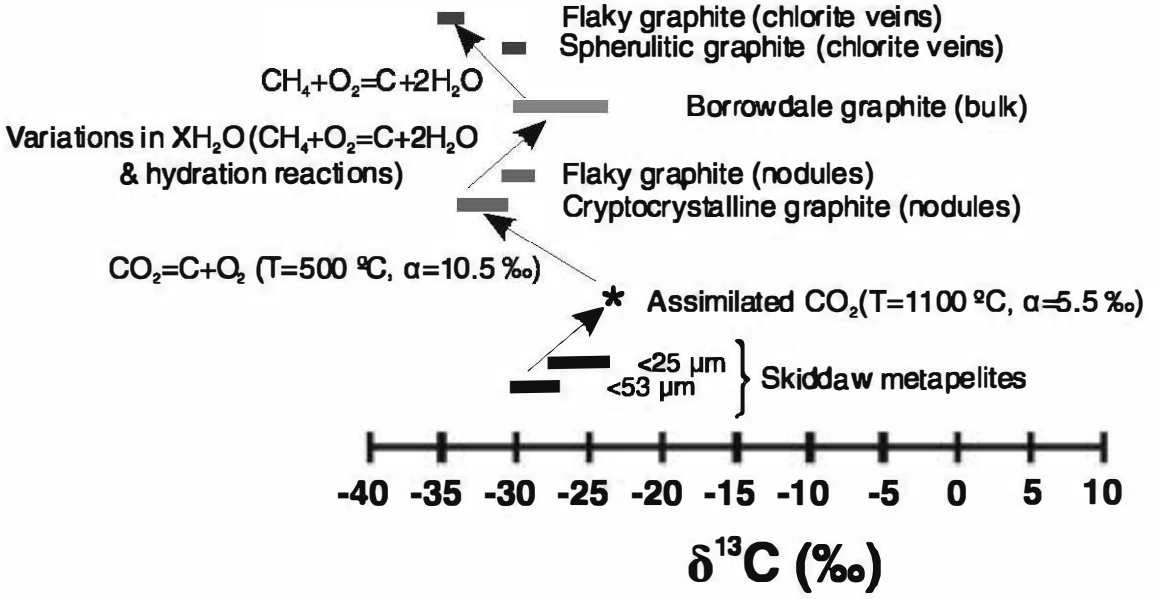

Fig. 14. Carbon stable isotope ratios of graphite from the Borrowdale deposit and of carbonaceous matter from Skiddaw Group metapelites. The figure outlines the fractionation of the original assimilated carbon as well as the reactions involved through the different stages of graphite deposition. The $\delta^{13}C$ values of individual graphite morphologies are those reported by Barrenechea et al. (2009).

gressively poorer in CO_2 (or richer in H_2O and CH_4 as CO_2 was being consumed in the graphite-generating reaction, see Fig. 13B) would lead to successive graphite crystals enriched in the heavy isotope (i.e. the flaky graphite within nodules, $\delta^{13}C = -30.2‰$; scenario, the hydration reactions of the host rocks during their coeval propylitic alteration could also contribute to the limited isotopic heterogeneity of graphite. Within the late chlorite–graphite veins, the morphologies corresponding to higher supersaturation (i.e. spherulites) are isotopically heavier than those formed under lower supersaturation (i.e. flakes). This trend suggests that graphite in the chlorite-graphite veins mainly crystallized following the reaction $CH_4 + O_2 \rightarrow C + 2H_2O$. In summary, the overall fluid system would have progressed towards the total consumption of CO_2 and most of the CH_4, as recorded by L1 inclusions with $\#XCO_2 \sim 0.03$ and by the latest L2 inclusion assemblage.

5.3. Controls on the emplacement of the graphite deposit

The key role of the hypabyssal dioritic intrusion in the emplacement of the Borrowdale graphite deposit is amply demonstrated by their close relationship, as shown first by Strens (1965). As previously mentioned, the BVG represents subaerial, subduction-related andesitic volcanism and associated high-level intrusions in which the assimilation of carbonaceous metapelitic rocks has been implicated (e.g. McConnell et al., 2002). In the volcanic environment, the carbonic species derived from the assimilation would be released during magma ascent, and transferred to the surface, probably through the fault network (Giammanco et al., 1998). There is growing evidence from melt inclusions that many magmas are vapour saturated at 10–15 km depth and that a significant proportion of this is CO_2 (Lowenstern, 2001; Wallace, 2005). According to Giggenbach (1996), volatile contents of andesitic magmas related to subduction zones (like the BVG) are likely to be high enough to allow a separate, volatile-rich phase to be present during all stages of magma generation and migration.

By contrast with the high-level volcanic setting, the crystallization of a batch of magma under subvolcanic-hypabyssal conditions at Seathwaite (i.e. the dioritic intrusion) provided a completely different scenario, with rapid magma ascent preventing the loss of the volatiles (mostly CO_2, CH_4 and H_2O) generated during assimilation. In the dioritic intrusion at Seathwaite, the crystallization of the primary anhydrous mineral assemblage (clinopyroxene, orthopyroxene and plagioclase; Strens, 1965) caused the residual magma to become enriched in volatiles. This led to an increase in the vapour pressure which eventually overcame the confining lithostatic pressure promoting the hydraulic fracturing (brecciation) of the host rock. In turn, the expansion of the volatiles triggered the upwards movement of andesitic and dioritic rocks and/or melt, quartz fragments, and a supercritical carbon-rich fluid (represented by the V inclusions) that resulted in the formation of the breccia pipe bodies. This C–O–H fluid remained metastable until the earliest hydration reactions triggered the nucleation of the first graphite crystals (spherulites and colloform aggregates). This initial stage was followed by massive precipitation of graphite coupled with the pervasive propylitic alteration of the host rocks. As previously discussed, the structural and isotopic evidence indicate that the whole mineralization process in Borrowdale was catastrophic, that is, it occurred in a geologically very short period of time.

Given the association with mafic intrusions, why is graphite mineralization restricted to the Seathwaite location? A significant number of hypabyssal mafic bodies of similar composition have been mapped throughout the Skiddaw Group outcrop to the north of Borrowdale (Fortey et al., 1994), yet none of these is known to have associated graphite deposits, nor have the few intrusions of this type that occur within the BVG outcrop (British Geological Survey 1:50,000-scale bedrock geological sheets 29, Keswick, and 38, Ambleside, 1999 and 1996, respectively). The answer may be the unique location of the Borrowdale intrusion in the immediate hanging wall of the Burtness Comb Fault (Fig. 1). This E- to ENE-striking fault with hade to the south, is inferred to lie above a repeatedly reactivated, deep-seated basement structure, and hence was one of the fundamental faults that controlled accumulation and preservation of the BVG (Millward, 2002). The fault may in part also mark the northern margin of the Scafell Caldera, a major piecemeal, hydrovolcanic system within the BVG (Branney and Kokelaar, 1994). Furthermore, faults with the same orientation as the graphite–chlorite veins at Seathwaite are known to have been involved in the volcanotectonic formation within the central part of the Scafell Caldera. Such active fault systems would have provided the necessary channel ways for the rapid ascent of both magma and C–O–H fluids.

6. CONCLUSIONS

The graphite deposit at Borrowdale is a unique type of mineralization in many aspects. Volcanic environments do not usually provide suitable conditions for the formation of volumetrically large graphite deposits. For this deposit to be formed an unusual combination of geological factors therefore occurred, including (1) the assimilation of carbonaceous matter by andesite magmas, (2) the existence of hypabyssal dioritic intrusions that prevented the loss of volatiles generated during assimilation as commonly occurs in volcanic environments, and (3) the singular occurrence at Seathwaite of one of these intrusions in the vicinity of an active deep-seated fault system, which provided the channelways for the flow of the C–O–H fluids.

The importance of tectonic control on the mineralization is emphasized further by the occurrence of graphite within near-vertical pipe-like bodies developed at the intersection of conjugate normal fractures which are also mineralized. Graphite mineralization and propylitic alteration of the volcanic host rocks in the Borrowdale deposit were intimately related. Both processes appear to have occurred in a short period of time. The mineralized breccia pipe bodies suggest a quick upwards transport of overpressured fluids, similar to diatreme-like bodies. The homogeneous carbon isotopic signature both at the microscale and at the scale of each single graphite nodule

also implies rapid deposition. Graphite precipitation started at ~500 °C and about 2 kbar from CO_2-rich fluids. The initial graphite precipitation was probably triggered by the earliest hydration reactions leading to chlorite formation. As mineralization proceeded, water-generating reactions were involved in graphite precipitation from fluids progressively richer in methane relative to carbon dioxide, thus resulting in the widespread propylitic alteration of the host rock. The ultimate source of carbon in the mineralizing fluids was the carbonaceous matter contained in the Skiddaw Group metapelites that were assimilated by the andesite magmas of the Borrowdale Volcanic Group.

ACKNOWLEDGEMENTS

We thank Dr. R. Rojas (Institute of Materials Science, Madrid), Dr. J. Alonso-Azcárate (Faculty of Environmental Sciences, University of Castilla-La Mancha), B. Soutullo (Dept. Cristalografía y Mineralogía, UCM), and A. Fernández-Larios (CAI Microscopía Electrónica Luis Bru, UCM) for technical assistance during DTA-TG, TOC, XRD, and EMPA analyses, respectively. We also acknowledge C. Valdehita for helping with the concentration of chlorite from chlorite graphite veins for the stable isotope studies. Dr. C. Brime kindly provided the reference samples for the KI calibration. We thank J.L.R. Touret and J.A.D. Connolly for helpful advice on the fluid inclusion relationships and on the stability of the propylitic assemblage, respectively. The paper was greatly improved from the revisions by K. Judik and two anonymous reviewers. Special thanks are due to Peter Ulmer (associate editor) for his excellent editorial handling and helpful comments. Thanks are also due to Jeff Wilkinson and Dave Bridge who took care of our safety during the underground work and guided us through the labyrinthine stages of the old graphite mine. The National Trust is also thanked for providing access to the mine. The graphite mine is both a Scheduled Ancient Monument and a Site of Special Scientific Interest: permission to collect samples there was granted by the Secretary of State for Culture, Media and Sport, and by Natural England, respectively. This paper is a contribution from Project CGL2006-00835 of the Spanish Ministry of Science and Innovation. David Millward publishes with the permission of the Executive Director, British Geological Survey (N.E.R.C.). This study was partly funded by INSU DyETI and ANR JC (GeoCarbons project) to Olivier Beyssac.

REFERENCES

Bakker R. J. (1997) CLATHRATES: computer programs to calculate fluid inclusion: V X. Properties using clathrate melting temperatures. *Comput. Geosci.* **23**, 1–18.

Bakker R. J. (1999) Adaptation of the Bowers and Helgeson (1983) equation of state to the H_2O CO_2 CH_4 N_2 NaCl system. *Chem. Geol.* **154**, 225–236.

Bakker R. J. (2003) Package FLUIDS 1. Computer programs for analysis of fluid inclusion data and for modelling bulk fluid properties. *Chem. Geol.* **194**, 3–23.

Bakker R. J. and Brown P. E. (2003) Computer modelling in fluid inclusion research. In *Fluid Inclusions: Analysis and Interpretation* (eds. I. Samson, A. Anderson and D. Marshall). Mineralogical Association of Canada, Short Course series **32**, pp. 175 212.

Barrenechea J. F., Luque F. J., Rodas M. and Pasteris J. D. (1997) Vein-type graphite mineralization in the Jurassic volcanic rocks of the external zone of the Betic Cordillera (Southern Spain). *Can. Mineral.* **35**, 1379–1390.

Barrenechea J. F., Luque F. J., Millward D., Ortega L., Beyssac O. and Rodas M. (2009) Graphite morphologies from the Borrowdale deposit (NW England, UK): Raman and SIMS data. *Contrib. Mineral. Petrol.* **158**, 37–51.

Bebout G. E., Cooper D. C., Bradley A. D. and Sadofsky S. J. (1999) Nitrogen-isotope record of fluid rock interactions in the Skiddaw aureole and granite, English Lake District. *Am. Mineral.* **84**, 1495–1505.

Beddoe-Stephens B., Petterson M. G., Millward D. and Marriner G. F. (1995) Geochemical variation and magmatic cyclicity within an Ordovician continental-arc volcanic field: the lower Borrowdale Volcanic Group, English Lake District. *J. Volcanol. Geotherm. Res.* **65**, 81–110.

Beyssac O., Goffé B., Chopin C. and Rouzaud J.-N. (2002) Raman spectra of carbonaceous material from metasediments: a new geothermometer. *J. Metamorphic Geol.* **20**, 859–871.

Beyssac O., Goffe B., Petitet J.-P., Froigneux E., Moreau M. and Rouzaud J.-N. (2003) On the characterization of disordered and heterogeneous carbonaceous materials by Raman spectroscopy. *Spectrochim. Acta Part A* **59**, 2267–2276.

Beyssac O., Bollinger L., Avouac J. P. and Goffé B. (2004) Thermal metamorphism in the lesser Himalaya of Nepal determined from Raman spectroscopy of carbonaceous material. *Earth Planet. Sci. Lett.* **225**, 233–241.

Binu-Lal S. S., Kehelpannala K. V. W., Satish-Kumar M. and Wada H. (2002) Multistage graphite precipitation through protracted fluid flow in sheared metagranitoid, Digana, Sri Lanka: evidence from stable isotopes. *Chem. Geol.* **197**, 253–270.

Bottinga Y. (1969) Calculated fractionation factors for carbon and hydrogen isotope exchange in the system calcite carbon dioxide graphite methane hydrogen water vapor. *Geochim. Cosmochim. Acta* **33**, 49–64.

Bowers T. S. and Helgeson H. C. (1983) Calculation of the thermodynamic and geochemical consequences of non-ideal mixing in the system H_2O CO_2 NaCl on phase relations in geologic systems; equation of state for H_2O CO_2 NaCl fluids at high pressures and temperatures. *Geochim. Cosmochim. Acta* **47**, 1247–1275.

Branney M. J. and Kokelaar B. P. (1994) Volcanotectonic faulting, soft-state deformation and rheomorphism of tuffs during development of a piecemeal caldera, English Lake District. *Geol. Soc. Am. Bull.* **106**, 507–530.

Buseck P. R. and Huang B. J. (1985) Conversion of carbonaceous material to graphite during metamorphism. *Geochim. Cosmochim. Acta* **49**, 2003–2016.

Cole D. R. and Ripley E. M. (1998) Oxygen isotope fractionation between chlorite and water from 170 to 350 °C: a preliminary assessment based on partial exchange and fluid/rock experiments. *Geochim. Cosmochim. Acta* **63**, 449–457.

Collins P. L. F. (1979) Gas hydrates in CO_2-bearingfluid inclusions and the use of freezing data for the estimation of salinity. *Econ. Geol.* **74**, 1435–1444.

Connolly J. A. D. (1990) Multivariable phase diagrams: an algorithm based on generalized thermodynamics. *Am. J. Sci.* **290**, 666–718.

Cooper A. H., Rushton A. W. A., Molyneux S. G., Hughes R. A., Moore R. M. and Webb B. C. (1995) The stratigraphy, correlation, provenance and paleogeography of the Skiddaw Group (Ordovician) in the English Lake District. *Geol. Mag.* **132**, 185–211.

Cooper A. H., ForteyN. J., Hughes R. A., Molyneux S. G., Moore R. M., Rushton A. W. A., Stone P., Allen P. M., Cooper D. C., Evans J. A., Hirons S. R. and Webb B. C. (2004) *The Skiddaw*

Group of the English Lake District.. Mem. British Geol. Surv., HMSO, London.

Cooper D. C., Lee M. K., Fortey N. J., Cooper A. H., Rundle C. C., Webb B. C. and Allen P. M. (1988) The Crummock Water aureole: a zone of metasomatism and source of ore metals in the English Lake District. *J. Geol. Soc. Lond.* **145**, 523–540.

Crespo E., Luque F. J., Fernández-Rodríguez C., Rodas M., Díaz-Azpiroz M., Fernández-Caliani J. C. and Barrenechea J. F. (2004) Significance of graphite occurrences in the Aracena Metamorphic Belt, Iberian Massif. *Geol. Mag.* **141**, 687–697.

Crespo E., Luque F. J., Barrenechea J. F. and Rodas M. (2006) Influence of grinding on graphite crystallinity from experimental and natural data: implications for graphite thermometry and sample preparation. *Mineral. Mag.* **70**, 697–707.

Duan Z., Møller N. and Weare J. H. (1992a) An equation of state for the CH_4 CO_2 H_2O system: I. Pure systems from 0 to 1000 °C and 0 to 8000 bar. *Geochim. Cosmochim. Acta* **56**, 2605–2617.

Duan Z., Møller N. and Weare J. H. (1992b) An equation of state for the CH_4 CO_2 H_2O system: II. Mixtures from 50 to 1000 °C and 0 to 1000 bar. *Geochim. Cosmochim. Acta* **56**, 2619–2631.

Dubessy J., Poty B. and Ramboz C. (1989) Advances in C O H N S fluid geochemistry based on micro-Raman spectrometric analysis of fluid inclusions. *Eur. J. Mineral.* **1**, 517–534.

Duke E. F., Galbreath K. C. and Trusty K. J. (1990) Fluid inclusion and carbon isotope studies of quartz graphite veins, Black Hills, South Dakota and Ruby Range, Montana. *Geochim. Cosmochim. Acta* **54**, 683–698.

Duke E. F. and Rumble D. (1986) Textural and isotopic variations in graphite from plutonic rocks, South-Central New Hampshire. *Contrib. Mineral. Petrol.* **93**, 409–419.

Farquhar J., Hauri E. and Wang J. (1999) New insights into carbon fluid chemistry and graphite precipitation: SIMS analysis of granulite facies graphite from Ponmudi, South India. *Earth Planet. Sci. Lett.* **171**, 607–621.

Ferry J. M. and Burt D. M. (1982) Characterization of metamorphic fluid composition thorough mineral equilibria. In *Characterization of metamorphism thorough mineral equilibria* (ed. J. M. Ferry). Mineralogical Society of America. *Rev. Mineral.* **10**, 207 262.

Fitton J. G. (1972) The genetic significance of almandine-pyrope phenocrysts in the calc-alkaline Borrowdale Volcanic Group, northern England. *Contrib. Mineral. Petrol.* **36**, 231–248.

Fortey N. J. (1989) Low grade metamorphism in the Lower Ordovician Skiddaw Group of the Lake District, England. *Proc. Yorks. Geol. Soc.* **47**, 325–337.

Fortey N. J., Roberts B. and Hirons S. R. (1993) Relationship between metamorphism and structure in the Skiddaw Group, English Lake District. *Geol. Mag.* **130**, 631–638.

Fortey N. J., Cooper A. H., Henney P. J., Colman T. and Nancarrow P. H. A. (1994) Appinitic intrusions in the English Lake District. *Mineral. Petrol.* **51**, 355–375.

French B. M. (1966) Some geological implications of equilibrium between graphite and a C O H gas at high temperatures and pressures. *Rev. Geophys.* **4**, 223–253.

Frost B. R. (1979) Mineral equilibria involving mixed-volatiles in a C O H fluid phase: the stabilities of graphite and siderite. *Am. J. Sci.* **279**, 1033–1059.

Galy V., Beyssac O., France-Lanord C. and Eglinton T. (2008) Selective recycling of graphite during Himalayan erosion: a geological stabilisation of C in the crust. *Science* **322**, 943–945.

Giammanco S., Gurrieri S. and Valenza M. (1998) Anomalous soil CO_2 degassing in relation to faults and eruptive fissures on Mount Etna (Sicily, Italy). *Bull. Volcanol.* **60**, 252–259.

Giggenbach W. F. (1996) Chemical composition of volcanic gases. In *Monitoring and Mitigation of Volcano Hazards* (eds. R. Scarpa and R. I. Tilling). Springer-Verlag, Berlin, pp. 221–256.

Giggenbach W. F., Shinohara H., Kusakabe M. and Ohba T. (2003) Formation of acid volcanic brines through interaction of magmatic gases, seawater, and rock within the White Island volcanic-hydrothermal system, New Zealand. In *Volcanic, Geothermal, and Ore-forming Fluids; Rulers and Witnesses of Processes within the Earth* (eds. S. F. Simmons and I. Graham). Special Publication, Society of Economic Geologists **10**, pp. 19 40.

Graham C. M., Viglino J. A. and Harmon R. S. (1987) Experimental study of hydrogen isotope exchange between aluminous chlorite and water and of hydrogen diffusion in chlorite. *Am. Mineral.* **72**, 566–579.

Grew E. S. (1974) Carbonaceous material in some metamorphic rocks of New England and other areas. *J. Geol.* **82**, 5–73.

Hedenquist J. W. and Aoki M. (1991) Meteoric interaction with magmatic discharges in Japan and the significance for mineralization. *Geology* **19**, 1041–1044.

Hedenquist J. W. and Lowenstern J. B. (1994) The role of magmas in the formation of hydrothermal ore deposits. *Nature* **370**, 519–527.

Hedenquist J. W., Matsuhisa Y., Izawa E., White N. C., Giggenbach W. F. and Aoki M. (1994) Geology, geochemistry, and origin of high sulfidation Cu Au mineralization in the Nansatsu District. *Jpn. Econ. Geol.* **89**, 1–30.

Henley R. W. and Hedenquist J. W. (1986) Introduction to the geochemistry of active and fossil geothermal system. In *Guide to the Active Epithermal (Geothermal) System and Precious Metal Deposits of New Zealand* (ed. P. J. Roberts). *Monograph Series on Mineral Deposits* **26**, pp. 1 22.

Holland T. J. B. and Powell R. (1998) An internally consistent thermodynamic data set for phases of petrological interest. *J. Metamorph. Geol.* **16**, 309–343.

Huizenga J.-M. (2005) COH, an Excel spreadsheet for composition calculations in the C O H fluid system. *Comput. Geosci.* **31**, 797–800.

Jarosewich E., Nelen J. A. and Norberg J. A. (1980) Reference samples for electron microprobe analysis. *Geostand. Newslett.* **4**, 43–47.

Judik K., Rantitsch G., Rainer T. M., Árkai P. and Tomljenović B. (2008) Alpine metamorphism of organic matter in metasedimentary rocks from Mt. Medvednica (Croatia). *Swiss J. Geosci.* **101**, 605–616.

Kisch H. J., Árkai P. and Brime C. (2004) On the calibration of the illite Kübler index (illite "crystallinity"). *Schweiz. Mineral. Petrogr. Mitt.* **84**, 323–331.

Kreulen R. (1987) Thermodynamic calculations of the C O H system applied to fluid inclusions: are fluid inclusions unbiased samples of ancient fluids? *Chem. Geol.* **61**, 59–64.

Kribek B., Hrabal J., Landais P. and Hladikova J. (1994) The association of poorly ordered graphite, coke and bitumens in greenschist facies rocks of the Ponikla' group, Lugikum, Czech Republic: the result of graphitization of various types of carbonaceous matter. *J. Metamorph. Geol.* **12**, 493–503.

Lee M. K. (1986) A new gravity survey of the Lake District and three-dimensional model of the granite batholith. *J. Geol. Soc. Lond.* **143**, 425–436.

Lindgren P. and Parnell J. (2006) Petrographic criteria for fluid mobility of graphitic carbon in terrestrial and extraterrestrial samples. *J. Geochem. Explor.* **91**, 126–129.

Liou J. G. (1993) Stabilities of natural epidotes. In *Proceedings of the 125 Jahre Kappenwand Symposium* (eds. V. Hock and F. Koller), Vienna, pp. 7 16.

Lowenstern J. B. (2001) Carbon dioxide in magmas and implications for hydrothermal systems. *Mineral. Deposita* **36**, 490–502.

Lowry D., Boyce A. J., Pattrick R. A. D., Fallick A. E. and Stanley C. J. (1991) A sulphur isotopic investigation of the potential

sulphur sources for Lower Palaeozoic-hosted vein mineralization in the English Lake District. *J. Geol. Soc. Lond.* **148**, 993–1004.

Luque F. J., Pasteris J. D., Wopenka B., Rodas M. and Barrenechea J. F. (1998) Natural fluid-deposited graphite: mineralogical characteristics and mechanisms of formation. *Am. J. Sci.* **298**, 471–498.

Luque F. J., Ortega L., Barrenechea J. F., Millward D., Beyssac O. and Huizenga J.-M. (2009) Deposition of highly crystalline graphite from moderate-temperature fluids. *Geology* **37**, 275–278.

McConnell B. J., Menuge J. F. and Hertogen J. (2002) Andesite petrogenesis in the Ordovician Borrowdale Volcanic Group of the English Lake District by fractionation, assimilation and mixing. *J. Geol. Soc. Lond.* **159**, 417–424.

Merriman R. J. (2006) Clay mineral assemblages in British Lower Palaeozoic mudrocks. *Clay Min.* **41**, 473–512.

Millward D. (2002) Early Palaeozoic magmatism in the English Lake District. *Proc. Yorks. Geol. Soc.* **54**, 65–93.

Millward D. (2004) The Caradoc volcanoes of the English Lake District. *Proc. Yorks. Geol. Soc.* **55**, 73–105.

Millward D. and Evans J. A. (2003) U Pb chronology of late Ordovician magmatism in the English Lake District. *J. Geol. Soc. Lond.* **160**, 773–781.

Mitchell J. G. and Ineson P. R. (1975) Potassium argon ages from the graphite deposits and related rocks of Seathwaite, Cumbria. *Proc. Yorks. Geol. Soc.* **40**, 413–418.

Murphy P. J. and Roberts S. (1995) Laser Raman spectroscopy of differential partitioning in mixed-gas clathnrtes in H_2O CO_2 N_2 fluid inclusions: Implications for microthermometry. *Geochim. Cosmochim. Acta* **59**, 4809–4824.

Ohmoto H. and Kerrick D. (1977) Devolatilization equilibria in graphitic systems. *Am. J. Sci.* **277**, 1031–1044.

Okuyama-Kusunose Y. and Itaya T. (1987) Metamorphism of carbonaceous material in the Tono contact aureole, Kitagami Mountains, Japan. *J. Metamorph. Geol.* **5**, 121–139.

Parnell J. (1982) Genesis of the graphite deposit at Seathwaite in Borrowdale, Cumbria. *Geol. Mag.* **119**, 511–512.

Ramboz C., Pichavant M. and Weisbrod A. (1982) Fluid inmiscibility in natural processes. Use and misuse of fluid inclusion data. II. Interpretation of fluid inclusion data in terms of immiscibility. *Chem. Geol.* **37**, 29–48.

Rantitsch G., Grogger W., Teichert C., Ebner F., Hofer C., Maurer E.-M., Schaffer B. and Toth M. (2004) Conversion of carbonaceous material to graphite within the Greywacke Zone of the Eastern Alps. *Int. J. Earth Sci.* **93**, 959–973.

Roedder E. (1984) *Fluid Inclusions* (ed. P. H. Ribbe). *Rev. Mineral.* **12**. Mineral. Soc. Am.

Rumble D., Duke E. F. and Hoering T. C. (1986) Hydrothermal graphite in New Hampshire: evidence of carbon mobility during regional metamorphism. *Geology* **14**, 452–455.

Santosh M., Wada H., Satish-Kumar M. and Binu-Lal S. S. (2003) Carbon isotope "stratigraphy" in a single graphite crystal; implications for the crystal growth mechanism of fluid-deposited graphite. *Am. Mineral.* **88**, 1689–1696.

Satish-Kumar M. (2005) Graphite-bearing CO_2 fluid inclusions in granulites: insights on graphite precipitation and carbon isotope evolution. *Geochim. Cosmochim. Acta* **69**, 3841–3856.

Scheele N. and Hoefs J. (1992) Carbon isotope fractionation between calcite, graphite and CO_2: an experimental study. *Contrib. Mineral. Petrol.* **112**, 35–45.

Sharp Z. D. (1990) Laser-based microanalytical method for the in situ determination of oxygen isotope ratios of silicates and oxides. *Geochim. Cosmochim. Acta* **54**, 1353–1357.

Sheppard S. M. F. (1986) Characterization and isotopic variations in natural waters. In *Stable Isotopes in High Temperature Geological Processes* (eds. J. W. Valley, H. P. J. Taylor and J. R. O'Neil). *Rev. Mineral.* **16**, 165 185.

Shi P. and Saxena S. K. (1992) Thermodynamic modelling of the C O H S fluid system. *Am. Mineral.* **77**, 1038–1049.

Soper N. J. and Woodcock N. H. (2003) The lost Lower Old Red Sandstone of England and Wales: a record of post-Iapetan flexure or Early Devonian transtension? *Geol. Mag.* **140**, 627–647.

Stone P., Cooper A. H. and Evans J. A. (1999) The Skiddaw Group (English Lake District) reviewed: early Palaeozoic sedimentation and tectonism at the northern margin of Avalonia. In *In Sight of the Suture: the Geology of the Isle of Man in its Iapetus Ocean Context* (eds. N. H. Woodcock, W. R. Fitches, D. G. Quirk and R. P. Barnes). Special Publication 160, Geological Society, London. pp. 325 336.

Strens R. G. J. (1965) The graphite deposit of Seathwaite in Borrowdale, Cumberland. *Geol. Mag.* **102**, 393–406.

Valley J. W., Kitchen N., Kohn M. J., NiendorfC. R. and Spicuzza M. J. (1995) UWG-2, a garnet standard for oxygen isotope ratios: Strategies for high precision and accuracy with laser heating. *Geochim. Cosmochim. Acta* **59**, 5223–5231.

Van den Kerkhof A. M., Touret J. L. R., Maijer C. and Jansen J. B. H. (1991) Retrograde methane-dominated fluid inclusions from high-temperature granulites of Rogaland, southwestern Norway. *Geochim. Cosmochim. Acta* **55**, 2533–2544.

Wada H., Tomita T., Matsuura K., Iuchi K., Ito M. and Morikiyo T. (1994) Graphitization of carbonaceous matter during metamorphism with references to carbonate and pelitic rocks of contact and regional metamorphisms. *Contrib. Mineral. Petrol.* **118**, 217–228.

Wallace P. J. (2005) Volatiles in subduction zone magmas: concentrations and fluxes based on melt inclusion and volcanic gas data. *J. Volcanol. Geotherm. Res.* **140**, 217–240.

Ward J. C. (1876) *The geology of the northern part of the English Lake District. Memoir of the Geological Survey of Great Britain.* Quarter Sheet 101SE (England and Wales Sheet 29, Keswick).

Weis P. L., Friedman I. and Gleason J. P. (1981) The origin of epigenetic graphite: evidence from isotopes. *Geochim. Cosmochim. Acta* **45**, 2325–2332.

Associate editor: Peter Ulmer